PHYSICAL REVIEW D **89,** 054015 (2014)

NLO twist-3 contribution to the pion electromagnetic form factors in k_T factorization

Shan Cheng, Ying-Ying Fan, and Zhen-Jun Xiao*

Department of Physics and Institute of Theoretical Physics, Nanjing Normal University, Nanjing, Jiangsu 210023, People's Republic of China

(Received 21 January 2014; published 17 March 2014)

In this paper, by employing the k_T factorization theorem, we calculate first the next-to-leading-order (NLO) twist-3 contributions to the pion electromagnetic form factors in the $\pi\gamma^* \to \pi$ process. From the analytical and numerical calculations we find the following points: (a) for the leading-order (LO) twist-2, twist-3, and the NLO twist-2 contributions, our results agree very well with those obtained in previous works, (b) we extract out two factors $F_{\mathrm{T3}}^{(1)}(x_i, t, Q^2)$ and $\bar{F}_{\mathrm{T3}}^{(1)}(x_i, t, Q^2)$, which describe directly the NLO twist-3 contributions to the pion electromagnetic form factors $F^+(Q^2)$, (c) the NLO twist-3 contribution is negative in sign and cancels partially with the NLO twist-2 part, so the total NLO contribution can therefore provide a roughly $\pm 20\%$ corrections to the total LO contribution in the considered ranges of Q^2, and (d) the theoretical predictions for $Q^2F^+(Q^2)$ in the low-Q^2 region agree well with currently available data, which can be improved by the inclusion of the NLO contributions.

DOI: 10.1103/PhysRevD.89.054015 PACS numbers: 12.38.Bx, 12.38.Cy, 12.39.St, 13.20.He

I. INTRODUCTION

The perturbative QCD (pQCD) factorization approach, based on the k_{T} factorization theorem [1–3], has been used to deal with the inclusive and exclusive processes [4–7]. In the k_{T} factorization theorem, the end-point singularities are removed by the small but nonzero transverse momentum k_{T} of the parton propagators. For many years, the application of the k_T factorization theorem was mainly at the leading-order (LO) level. But the situation changed a lot recently. In Refs. [8–10], the authors calculated the next-to-leading-order (NLO) twist-2 contributions to the π transition form factor, π electromagnetic form factor and $B \to \pi$ form factor respectively, obtained the infrared finite k_T dependent NLO hard kernel, and therefore confirmed the applicability of the k_T factorization to these exclusive processes at the NLO and the leading twist (twist-2) level. This fact tell us that the k_T factorization approach can also be applied to the high-order contributions as mentioned in Ref. [11].

In the framework of the pQCD factorization approach, the contributions to the form factors include four parts.

(i) The leading-order contribution includes the leading-order twist-2 (LO-T2) contribution and the leading-order twist-3 (LO-T3) contribution.

(ii) The NLO contribution contains the NLO twist-2 (NLO-T2) contribution and the NLO twist-3 (NLO-T3) contribution.

At present, the first three parts, namely the LO-T2, LO-T3, and NLO-T2 contributions, have been evaluated in Refs. [8–10], but the NLO-T3 contribution is still absent now.

At leading-order level, the LO-T2 part is smaller than the LO-T3 part, by a ratio of ~34% against ~66% as shown in Refs. [9,12,13]. The NLO-T2 part is around 20%–30% of the total leading-order contribution (i.e., LO-T2 plus LO-T3 part) in the low Q^2 region. Since the LO-T3 contribution is large, the remaining unknown fourth part, the NLO twist-3 contribution, may be rather important and should be calculated in order to obtain the pQCD predictions for relevant form factors at the full NLO level, and to demonstrate that the k_T factorization theorem is an systematical tool.

In this paper we concentrate on the calculation for the NLO twist-3 contribution to the π electromagnetic form factor, which corresponds to the scattering process $\pi\gamma^\star \to \pi$. Our work represents the first calculation for the NLO twist-3 contribution to this quantity in the k_T factorization theorem.

We know that the collinear divergences would appear when the massless gluon is emitted from the light external line as the gluon is parallel to the initial- or the final-state pion which are assumed to be massless. The soft divergences would come from the exchange of the massless gluon between two on-shell external lines. In this work light partons are considered to be off-shell by k_T^2 to regulate the infrared divergences in both the QCD quark diagrams and the effective diagrams for pion wave functions. It's a nontrivial work to verify that the collinear divergences from the quark-level diagrams offset those from the pion wave functions and the soft divergences cancel among quark-level diagrams exactly at the twist-3 level as well as at the leading twist-2 case [9]. As demonstrated in Refs. [9,10], both the large double logarithms $\alpha_s \ln^2(k_T)$ and $\alpha_s \ln^2(x_i)$, here with x_i being the parton momentum fraction of the

*xiaozhenjun@njnu.edu.cn

antiquark in the meson wave functions, could be absorbed through the resummation technology. The double logarithm $\alpha_s \ln^2(k_T)$ would be absorbed into the π meson wave functions and then been summed to all orders in the coupling constant α_s by the k_T resummation [3]. The jet function would be included when exist the end-point singularity in the hard kernel, and then the double logarithm $\alpha_s \ln^2(x_i)$ would be summed to all orders by the threshold resummation [14–16]. The renormalization scale μ and the factorization scale μ_f are introduced in the high-order corrections to the QCD quark diagrams and the effective diagrams, respectively. With the appropriate choice of the scale μ and μ_f, say setting them as the internal hard scale as postulated in [9], the NLO corrections are under control.

This paper is organized as follows. In Sec. II, we give a brief review about the evaluations of the LO diagrams for the process $\pi\gamma^* \to \pi$, for both the twist-2 part and twist-3 part. In Sec. III, $O(\alpha_s^2)$ QCD quark diagrams for the process will be calculated with the inclusion of the twist-3 contributions. The convolutions of $O(\alpha_s)$ (NLO) effective diagrams for the meson wave functions and $O(\alpha_s)$ (LO) hard kernel would also be presented in this section, then the k_T-dependent NLO hard kernel at twist-3 will be obtained. Section IV contains the numerical analysis. With appropriate choices for the renormalization scale μ, the factorization scale μ_f and the input meson wave functions, we make the numerical calculations for all four parts of the LO and NLO contributions to the pion electromagnetic form factor in the $\pi\gamma^* \to \pi$ process. Section V contains the conclusions.

II. LO TWIST-2 AND TWIST-3 CONTRIBUTIONS

The leading-order hard kernels of the π electromagnetic form factor as shown in Fig. 1 are calculated in this section. The $\pi\gamma^\star \to \pi$ form factors are defined via the matrix element

$$\langle \pi(p_2)|J^\mu|\pi(p_1)\rangle = f_1(q^2)p_1^\mu + f_2(q^2)p_2^\mu = F^+(q^2)(p_1^\mu + p_2^\mu), \quad (1)$$

where p_1 (p_2) refers to the momentum of the initial (final) state pion, $q = p_1 - p_2$ is the momentum transferred in the weak vertex. Using the same definitions for the leading case as being used in Ref. [9], the momentum p_1 and p_2 are chosen as

$$p_1 = (p_1^+, 0, \mathbf{0}_\mathrm{T}), \quad p_2 = (0, p_2^-, \mathbf{0}_\mathrm{T}), \quad (2)$$

with $q^2 = -2p_1 \cdot p_2 = -Q^2$. According to the k_T factorization, $k_1 = (x_1 p_1^+, 0, k_{1\mathrm{T}})$ in the initial pion meson and $k_2 = (0, x_2 p_2^-, k_{2\mathrm{T}})$ in the final pion meson as labeled in Fig. 1, and x_1 and x_2 are the momentum fractions. The following hierarchy is postulated in the small-x region,

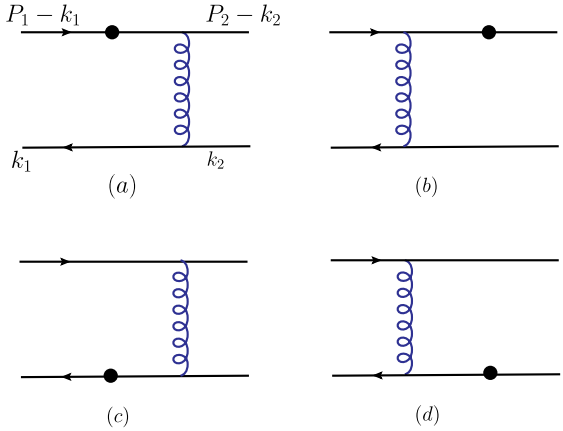

FIG. 1 (color online). Leading-order quark diagrams for the $\pi\gamma^\star \to \pi$ form factor with the symbol (filled circle) representing the virtual photon vertex.

$$Q^2 \gg x_2 Q^2 \sim x_1 Q^2 \gg x_1 x_2 Q^2 \gg k_{1T}^2, k_{2T}^2, \quad (3)$$

The following Fierz identity is employed to factorize the fermion flow:

$$I_{ij}I_{lk} = \frac{1}{4}I_{ik}I_{lj} + \frac{1}{4}(\gamma_5)_{ik}(\gamma_5)_{lj} + \frac{1}{4}(\gamma^\alpha)_{ik}(\gamma^\alpha)_{lj} + \frac{1}{4}(\gamma_5\gamma^\alpha)_{ik}(\gamma_\alpha\gamma_5)_{lj} + \frac{1}{8}(\sigma^{\alpha\beta}\gamma_5)_{ik}(\sigma_{\alpha\beta}\gamma_5)_{lj}. \quad (4)$$

The identity matrix I here is a four-dimensional matrix, the structure $\gamma_\alpha\gamma_5$ in Eq. (4) contributes at the leading twist (twist-2), while γ_5 and $\sigma_{\alpha\beta}\gamma_5$ contribute at the twist-3 level. The identity of the $SU(3)_c$ group,

$$I_{ij}I_{lk} = \frac{1}{N_c}I_{lj}I_{ik} + 2(T^c)_{lj}(T^c)_{ik} \quad (5)$$

is also employed to factorize the color flow. In Eq. (5), (i, j, l, k) are the color index, $N_c = 3$ is the number of the colors, and T^c is the Gel-Mann color matrix of $SU(3)_c$. The first term in Eq. (5) corresponds to the color-singlet state of the valence quark and the antiquark, while the second term will be associated with the color-octet state.

We here consider only the subdiagram Fig. 1(a) in detail, where the quark and antiquark form a color-singlet state. The hard kernels of the other subdiagrams can be obtained by simpe kinetic replacements. The wave function $\Phi_\pi(p_i, x_i)$ for the initial and final state pion can be written as the following form [17–19],

$$\Phi_\pi(p_1, x_1) = \frac{i}{\sqrt{2N_c}}\gamma_5\{\not{p}_1\phi_\pi^A(x_1) + m_0[\phi_\pi^P(x_1) - (\not{n}_+\not{n}_- - 1)\phi_\pi^T(x_1)]\}, \quad (6)$$

$$\Phi_\pi(p_2,x_2)=\frac{i}{\sqrt{2N_c}}\gamma_5\{\not p_2\phi_\pi^A(x_2) + m_0[\phi_\pi^P(x_2)-(\not n_-\not n_+-1)\phi_\pi^T(x_2)]\}, \quad (7)$$

where $n_+=(1,0,\mathbf{0}_\mathrm{T})$ and $n_-=(0,1,\mathbf{0}_\mathrm{T})$ denote the unit vector along with the positive and negative z-axis direction, $m_0=1.74$ GeV is the chiral mass of pion, N_c is the number of colors, $\phi_\pi^A(x_i)$ are the leading twist-2 pion distribution amplitudes, while $\phi_\pi^P(x_i)$ and $\phi_\pi^T(x_i)$ are the twist-3 pion distribution amplitudes.

Combining the decompositions in Eqs. (4) and (5), we then can sandwich Fig. 1(a) with the structures

$$\frac{1}{4N_c}\not p_1\gamma_5, \quad \frac{1}{4N_c}\gamma_5\not p_2 \quad (8)$$

from the initial and final state, respectively, in order to obtain the hard kernel $H^{(0)}$ at twist-2 level. For the derivation of the twist-3 hard kernel, one should sandwich Fig. 1(a) with the following two sets of structures:

$$\left(\frac{1}{4N_c}\gamma_5,\ \frac{1}{4N_c}\gamma_5\right);\quad \left(\frac{1}{8N_c}\sigma^{\alpha\beta}\gamma_5,\ \frac{1}{8N_c}\sigma_{\alpha\beta}\gamma_5\right). \quad (9)$$

Then the LO twist-3 contribution to the hard kernel from Fig. 1(a) can be written as [20]

$$H_a^{(0)}(x_1,k_{1\mathrm{T}},x_2,k_{2\mathrm{T}})=(-2ie_q)4\pi\alpha_s\frac{C_F}{16N_c}m_0^2\phi_\pi^P(x_2)\cdot\left\{\frac{-4p_2^\mu[\phi_\pi^P(x_1)-\phi_\pi^T(x_1)]}{(p_2-k_1)^2(k_1-k_2)^2} + \frac{4x_1p_1^\mu[\phi_\pi^P(x_1)+\phi_\pi^T(x_1)]}{(p_2-k_1)^2(k_1-k_2)^2}\right\}, \quad (10)$$

where α_s is the strong coupling constant, $C_F=4/3$ is the color factor, and e_q refers to the charge of the quark interacting with the γ^* in the $\pi\gamma^*\to\pi$ process.

The corresponding LO twist-2 contribution to the hard kernel takes the form of

$$H_{\mathrm{a,T2}}^{(0)}(x_1,k_{1T},x_2,k_{2T})=(ie_q)4\pi\alpha_s\frac{C_F}{16N_c}Q^2\phi_\pi^A(x_2)\phi_\pi^A(x_1)\cdot\frac{4x_1p_1^\mu}{(p_1-k_2)^2(k_1-k_2)^2} \quad (11)$$

It is easy to see that all parts of the initial state pion, the twist-2 $\phi_\pi^A(x_1)$ and twist-3 $\phi_\pi^P(x_1)$ and $\phi_\pi^T(x_1)$, provide contributions at the leading-order level, but only the $\phi_\pi^A(x_2)$ and $\phi_\pi^P(x_2)$ of the final state pion contribute at the LO level, because the contribution from the $\phi_\pi^T(x_2)$ component becomes zero when it is contracting with the gluon propagator. For the LO twist-3 hard kernel $H_a^{(0)}(x_1,k_{1T},x_2,k_{2T})$, one can see that it contains two Lorentz structures: the p_2^μ term and $x_1p_1^\mu$ term, which both should be included in the numerical calculations. For the LO twist-2 hard kernel $H_{\mathrm{a,T2}}^{(0)}$ as given in Eq. (11), it depends on one term $x_1p_1^\mu$ only. From previous studies in Ref. [9,12,13], we know that the LO twist-2 part is only about half of the LO twist-3 part. So one generally expects that the NLO twist-3 contribution may be large and essential for considered transitions, which is also one of the motivations of this paper.

III. NLO CORRECTIONS

Under the hierarchy as shown in Eq. (3), only those terms that do not vanish in the limits of $x_i\to 0$ and $k_{iT}\to 0$ should be kept; this fact does simplify the expressions of the NLO contributions greatly.

From the discussions at the end of Sec. I, we know that both Lorentz structures $x_1p_1^\mu$ and p_2^μ will contribute. From the hard kernel $H_a^{(0)}(x_1,k_{1\mathrm{T}},x_2,k_{2\mathrm{T}})$ as given in Eq. (10), we define those two parts of the LO twist-3 contribution, $H_a^{(0)}(x_1p_1^\mu)$ and $H_a^{(0)}(p_2^\mu)$, as

$$H_a^{(0)}(x_1p_1^\mu)\equiv(-2ie_q)4\pi\alpha_s\frac{C_F}{16N_c}m_0^2\phi_\pi^P(x_2)\times\frac{4x_1p_1^\mu[\phi_\pi^P(x_1)-\phi_\pi^T(x_1)]}{(p_2-k_1)^2(k_1-k_2)^2}, \quad (12)$$

$$H_a^{(0)}(p_2^\mu)\equiv(-2ie_q)4\pi\alpha_s\frac{C_F}{16N_c}m_0^2\phi_\pi^P(x_2)\times\frac{-4p_2^\mu[\phi_\pi^P(x_1)+\phi_\pi^T(x_1)]}{(p_2-k_1)^2(k_1-k_2)^2}, \quad (13)$$

$$H_a^{(0)}=H_a^{(0)}(x_1p_1^\mu)+H_a^{(0)}(p_2^\mu). \quad (14)$$

For Figs. 1(b)–(d), one can find the corresponding LO twist-3 contributions by simple replacements. For the sake of simplicity, we will generally omit the subscript "a" in $H_a^{(0)}$ in the following sections, unless stated specifically.

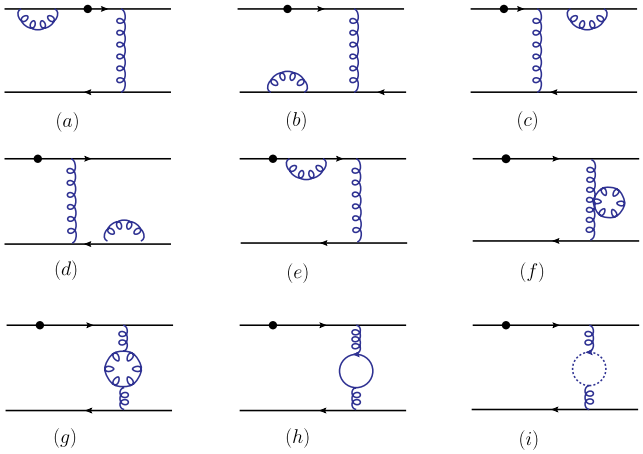

FIG. 2 (color online). Self-energy corrections to Fig. 1(a).

A. NLO twist-3 contributions of the QCD quark diagrams

Now we calculate the NLO twist-3 contributions to Fig. 1(a), which comes from the self-energy diagrams, the vertex diagrams, the box and the pentagon diagrams, as illustrated in Figs. 2, 3, and 4, respectively. After completing the calculations for Fig. 1(a), we can obtain the results for other three figures—Figs. 1(b)–(d)—by simple replacements.

The ultraviolet (UV) divergences are extracted in the dimensional reduction [21] in order to avoid the ambiguity from handing the matrix γ_5. The infrared (IR) divergences are identified as the logarithms $\ln\delta_1$, $\ln\delta_2$ and their combinations, as defined in Ref. [9],

$$\delta_1 = \frac{k_{1T}^2}{Q^2}, \quad \delta_2 = \frac{k_{2T}^2}{Q^2}, \quad \delta_{12} = \frac{-(k_1-k_2)^2}{Q^2}. \tag{15}$$

The self-energy corrections obtained by evaluating the one-loop Feynman diagrams in Figs. 2(a)–(f) are of the form

$$\begin{aligned}
G_{2a}^{(1)} &= -\frac{\alpha_s C_F}{8\pi}\left[\frac{1}{\varepsilon}+\ln\frac{4\pi\mu^2}{\delta_1 Q^2 e^{\gamma_E}}+2\right]H^{(0)},\\
G_{2b}^{(1)} &= -\frac{\alpha_s C_F}{8\pi}\left[\frac{1}{\varepsilon}+\ln\frac{4\pi\mu^2}{\delta_1 Q^2 e^{\gamma_E}}+2\right]H^{(0)},
\end{aligned} \tag{16}$$

$$\begin{aligned}
G_{2c}^{(1)} &= -\frac{\alpha_s C_F}{8\pi}\left[\frac{1}{\varepsilon}+\ln\frac{4\pi\mu^2}{\delta_2 Q^2 e^{\gamma_E}}+2\right]H^{(0)},\\
G_{2d}^{(1)} &= -\frac{\alpha_s C_F}{8\pi}\left[\frac{1}{\varepsilon}+\ln\frac{4\pi\mu^2}{\delta_2 Q^2 e^{\gamma_E}}+2\right]H^{(0)},\\
G_{2e}^{(1)} &= -\frac{\alpha_s C_F}{4\pi}\left[\frac{1}{\varepsilon}+\ln\frac{4\pi\mu^2}{x_1 Q^2 e^{\gamma_E}}+2\right]H^{(0)},\\
G_{2f+2g+2h+2i}^{(1)} &= \frac{\alpha_s}{4\pi}\left[\left(\frac{5}{3}N_c-\frac{2}{3}N_f\right)\left(\frac{1}{\varepsilon}+\ln\frac{4\pi\mu^2}{\delta_{12}Q^2e^{\gamma_E}}\right)\right]H^{(0)},
\end{aligned} \tag{17}$$

where $1/\varepsilon$ represents the UV pole term, μ is the renormalization scale, γ_E is the Euler constant, N_c is the number of quark color, N_f is the number of the active quarks flavors, and $H^{(0)}$ denotes the LO twist-3 hard kernel described in Eq. (10). Figures 2(f)–(i) denote the self-energy correction to the exchanged gluon.

It is easy to find that the NLO self-energy corrections to the LO twist-3 hard kernels as listed in Eqs. (16) and (17) are identical in form to those self-energy corrections to the LO twist-2 hard kernels as given in Eqs. (6)–(9) in Ref. [9]. The reason is that the self-energy diagrams don't involve the external lines and therefore are irrelevant with the twist structures of the wave functions. It should be note that an additional symmetry factor $\frac{1}{2}$ appeared from the choice of the gluon end point to attach the external line in the self-energy correction Figs. 2(a)–(d). The self-energy corrections to the external lines will be canceled by the corresponding effective diagrams as shown in Figs. (5) and (6). The self-energy correction to the internal quark line as shown in Fig. 2(e) does not generate any IR divergences.

The vertex corrections obtained by evaluating the one-loop Feynman diagrams in Figs. 3(a)–(e) are of the form

$$\begin{aligned}
G_{3a}^{(1)} &= \frac{\alpha_s C_F}{4\pi}\left[\frac{1}{\varepsilon}+\ln\frac{4\pi\mu^2}{Q^2e^{\gamma_E}}+\frac{1}{2}\right]H^{(0)},\\
G_{3b}^{(1)} &= -\frac{\alpha_s}{8\pi N_c}\left[\frac{1}{\varepsilon}+\ln\frac{4\pi\mu^2}{x_1Q^2e^{\gamma_E}}-1\right]H^{(0)}\\
&\quad -\frac{\alpha_s}{8\pi N_c}\left[1-\ln\frac{\delta_2}{x_1}\right]H^{(0)}(x_1p_1^\mu),\\
G_{3c}^{(1)} &= -\frac{\alpha_s}{8\pi N_c}\left[\frac{1}{\varepsilon}+\ln\frac{4\pi\mu^2}{\delta_{12}Q^2e^{\gamma_E}}\right]H^{(0)}\\
&\quad -\frac{\alpha_s}{8\pi N_c}\left[\ln\frac{\delta_2}{\delta_{12}}\ln\frac{\delta_1}{\delta_{12}}+\ln\frac{\delta_1}{\delta_{12}}+\ln\frac{\delta_2}{\delta_{12}}+\frac{\pi^2}{3}\right]H^{(0)}(p_2^\mu),\\
G_{3d}^{(1)} &= \frac{\alpha_s N_c}{8\pi}\left[\frac{3}{\varepsilon}+3\ln\frac{4\pi\mu^2}{\delta_{12}Q^2e^{\gamma_E}}+\frac{11}{2}\right]H^{(0)}\\
&\quad -\frac{\alpha_s N_c}{8\pi}\left[\ln\frac{\delta_1}{\delta_{12}}+\ln\frac{\delta_2}{\delta_{12}}\right]H^{(0)}(p_2^\mu)\\
G_{3e}^{(1)} &= \frac{\alpha_s N_c}{8\pi}\left[\frac{3}{\varepsilon}+3\ln\frac{4\pi\mu^2}{x_1Q^2e^{\gamma_E}}+\frac{11}{2}\right]H^{(0)}\\
&\quad -\frac{\alpha_s N_c}{8\pi}\left[\ln\frac{\delta_2}{x_1}\ln x_2+\ln\frac{\delta_2}{x_1}\right]H^{(0)}(x_1p_1^\mu).
\end{aligned} \tag{18}$$

It is easy to find that the NLO twist-3 corrections to the LO hard kernel $H^{(0)}$ in Eq. (14) have the UV divergence and they have the same divergence behavior in the self-energy and the vertex corrections. The summation of these UV divergences leads to the same result as the one for the NLO twist-2 case [9],

$$\frac{\alpha_s}{4\pi}\left(11-\frac{2}{3}N_f\right)\frac{1}{\varepsilon}, \tag{19}$$

which meets the requirement of the universality of the wave functions.

The amplitude $G_{3a}^{(1)}$ has no IR divergence due to the fact that the numerator in the amplitude of the collinear region is dominated by the transverse contributions which are negligible in Fig. 3(a). IR divergences in $G_{3c}^{(1)}$ and $G_{3d}^{(1)}$ are only relevant with the hard kernel $H^{(0)}(p_2^\mu)$, which is induced by the singular gluon attaches to the down quark lines. Similarly, IR divergences in $G_{3b}^{(1)}$ and $G_{3e}^{(1)}$ only occur in the hard kernel $H^{(0)}(x_1p_1^\mu)$ since the singular gluon is attached to the up quark lines.

The amplitude $G_{3b}^{(1)}$ should have collinear divergence because the radiative gluon in Fig. 3(b) is attached to the

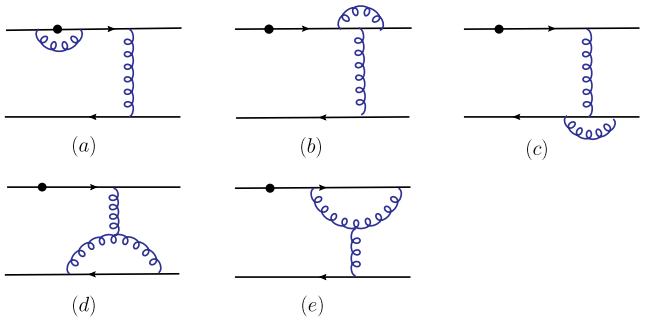

FIG. 3 (color online). Vertex corrections to Fig. 1(a).

light valence quark of the final state pion, and we find that the IR contribution is regulated by $\ln\delta_2$. Both the collinear and soft divergences are produced in $G_{3c}^{(1)}$ because the radiative gluon in Fig. 3(c) is attached to the external light valence antiquarks. The large double logarithm $\ln\delta_1\ln\delta_2$ comes from the overlap of the IR divergences, and will be canceled by the large double logarithm term from Fig. 4(f).

The radiative gluon in Fig. 3(d) is attached to the light valence anti-quarks as well as the virtual LO hard gluon, so the soft divergence and the large double logarithm aren't generated in $G_{3d}^{(1)}$. The radiative gluon in Fig. 3(e) is attached only to the light valence quark as well as the virtual LO hard gluon, and then $G_{3e}^{(1)}$ just contains the collinear divergence regulated by $\ln\delta_2$ in the $l\|P_2$ region.

The NLO twist-3 contributions from the box and pentagon diagrams as shown in Fig. 4 are summarized as

$$
\begin{aligned}
G_{4a}^{(1)} &= -\frac{\alpha_s N_c}{8\pi}\left[(1+\ln x_1)\ln\delta_1 - \left(1+\frac{3}{2}\ln x_1\right)\ln x_2 + \frac{1}{8}+\frac{\pi^2}{12}\right]H^{(0)}(x_1 p_1^\mu),\\
&\quad -\frac{\alpha_s N_c}{8\pi}\left[(1+\ln x_2)\ln\delta_2 - \left(1+\frac{3}{2}\ln x_2\right)\ln x_1 + \frac{1}{8}+\frac{\pi^2}{12}\right]H^{(0)}(x_2 p_2^\mu),\\
G_{4b}^{(1)} &\equiv 0,\\
G_{4c}^{(1)} &= -\frac{\alpha_s}{8\pi N_c}\left[\ln\frac{x_1}{\delta_2}\ln\frac{x_2}{\delta_1}+\ln^2 x_2\right]H^{(0)}(x_1 p_1^\mu) - \frac{\alpha_s}{8\pi N_c}\left[\ln\frac{x_2}{\delta_1}\ln\frac{x_1}{\delta_2}+\ln^2 x_1\right]H^{(0)}(x_2 p_2^\mu),\\
G_{4d}^{(1)} &\equiv 0,\\
G_{4e}^{(1)} &= \frac{\alpha_s}{8\pi N_c}\left[\ln\delta_1\ln\delta_2+\ln\delta_1+\frac{5}{4}\right]H^{(0)}(x_1 p_1^\mu),\\
G_{4f}^{(1)} &= -\frac{\alpha_s}{8\pi N_c}\left[\ln\frac{\delta_1}{\delta_{12}}\ln\frac{\delta_2}{\delta_{12}}-2\ln 2-1\right]H^{(0)}(p_2^\mu).
\end{aligned}
\tag{20}
$$

Because of the properties of the propagators in the above four- and five-point integrals, there is no UV divergence in the above amplitudes. Figures 4(b) and 4(d) are two-particle reducible diagrams; their contribution should be canceled by the corresponding effective diagrams, Figs. 5(c) and 6(c), for the NLO initial and final state meson wave functions due to the requirement of the factorization theorem, so we can set them to zero safely.

The $H^{(0)}(x_2 p_2^\mu)$ terms appearing in $G_{4a}^{(1)}$ and $G_{4c}^{(1)}$ are obtained from the evaluation of Figs. 4(a) and 4(c) only. The LO hard kernel $H^{(0)}(x_2 p_2^\mu)$ has the same form as the $H^{(0)}(x_1 p_1^\mu)$ as defined in Eq. (12) but with replacements of $x_1 \to x_2$ and $p_1^\mu \to p_2^\mu$. IR regulators only appear to the hard kernel $H^{(0)}(x_1 p_1^\mu)$ of Figs. 4(a)–(e), which are decided by the fact that the left end point of the emission gluon is attached to the up light external line. Similarly, Fig. 4(f)

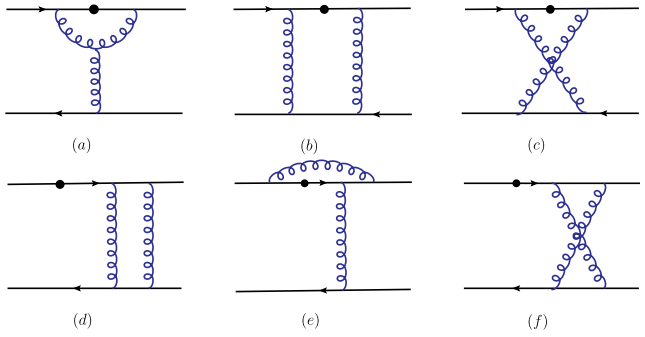

FIG. 4 (color online). Box and pentagon corrections to Fig. 1(a).

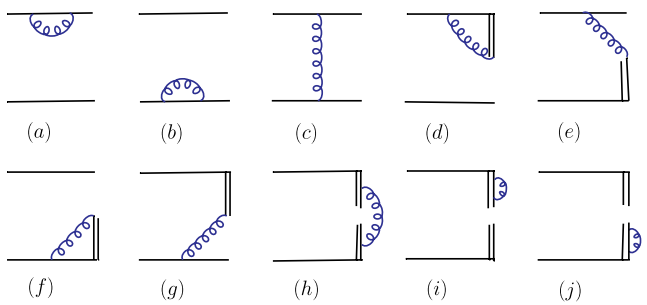

FIG. 5 (color online). The effective $O(\alpha_s)$ diagrams for the initial π meson wave function.

only grows the IR regulators to the hard kernel $H^{(0)}(p_2^\mu)$. Note that the emission gluon in Figs. 4(c), 4(e), and 4(f) is attached to external light lines, so its amplitude would dominate in the collinear region and soft region, and then the double logarithm would appear. The attaching of the emission gluon in Fig. 4(a) to the initial external line and the LO hard kernel reveals that only the IR regulator $\ln\delta_1$ is grown in the amplitude $G^{(1)}_{4a}$.

Now we just consider the IR parts regulated by $\ln\delta_i$, which would not be canceled directly by their counterparts from the effective diagrams of Fig. 5. These IR pieces appear in $G^{(1)}_{3b,3c,3d,3e}$ and $G^{(1)}_{4a,4c,4e,4f}$. We class these amplitudes into two sets according to the hard kernels to which those IR regulators $\ln\delta_i$ give corrections. Then the first set includes $G^{(1)}_{3c,3d}$ and $G^{(1)}_{4f}$, while the second set contains $G^{(1)}_{3b,3e}$ and $G^{(1)}_{4a,4c,4e}$ terms. These amplitudes are calculated in the leading IR regions to fit in with the k_T factorization theorem.

We firstly evaluate the NLO twist-3 corrections to $H^{(0)}(p_2^\mu)$. The amplitudes $G^{(1)}_{3c,3d}$ and $G^{(1)}_{4f}$ are recalculated by employing the phase space slicing method [22],

$$\begin{aligned}
G^{(1)}_{3c}(l\to 0) &= \frac{\alpha_s}{8\pi N_c}\left[\ln\frac{\delta_1}{\delta_{12}}\ln\frac{\delta_2}{\delta_{12}}+\frac{\pi^2}{3}\right]H^{(0)}(p_2^\mu),\\
G^{(1)}_{3c}(l\|p_1) &= \frac{\alpha_s}{8\pi N_c}\left[\ln\frac{\delta_1}{\delta_{12}}\ln\frac{\delta_2}{\delta_{12}}+\ln\frac{\delta_1}{\delta_{12}}\right]H^{(0)}(p_2^\mu),\\
G^{(1)}_{3c}(l\|p_2) &= \frac{\alpha_s}{8\pi N_c}\left[\ln\frac{\delta_1}{\delta_{12}}\ln\frac{\delta_2}{\delta_{12}}+\ln\frac{\delta_2}{\delta_{12}}\right]H^{(0)}(p_2^\mu),
\end{aligned}\tag{21}$$

$$\begin{aligned}
G^{(1)}_{3d}(l\|p_1) &= \frac{\alpha_s N_c}{8\pi}\left[-\ln\frac{\delta_1}{\delta_{12}}\right]H^{(0)}(p_2^\mu),\\
G^{(1)}_{3d}(l\|p_2) &= \frac{\alpha_s N_c}{8\pi}\left[-\ln\frac{\delta_2}{\delta_{12}}\right]H^{(0)}(p_2^\mu),
\end{aligned}\tag{22}$$

$$\begin{aligned}
G^{(1)}_{4f}(l\to 0) &= -\frac{\alpha_s}{8\pi N_c}\left[\ln\frac{\delta_1}{\delta_{12}}\ln\frac{\delta_2}{\delta_{12}}+\frac{\pi^2}{3}\right]H^{(0)}(p_2^\mu),\\
G^{(1)}_{4f}(l\|p_1) &= -\frac{\alpha_s}{8\pi N_c}\left[\ln\frac{\delta_1}{\delta_{12}}\ln\frac{\delta_2}{\delta_{12}}+\frac{\pi^2}{6}-1\right]H^{(0)}(p_2^\mu),\\
G^{(1)}_{4f}(l\|p_2) &= -\frac{\alpha_s}{8\pi N_c}\left[\ln\frac{\delta_1}{\delta_{12}}\ln\frac{\delta_2}{\delta_{12}}+\frac{\pi^2}{6}-2\ln 2\right]H^{(0)}(p_2^\mu).
\end{aligned}\tag{23}$$

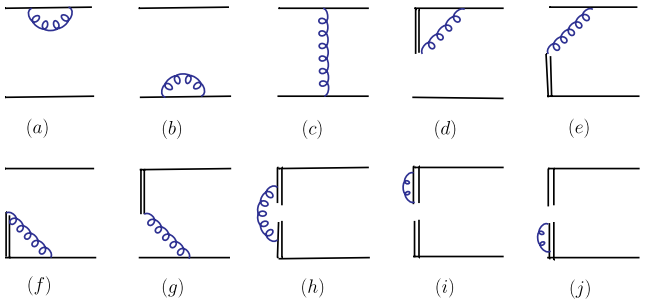

FIG. 6 (color online). The $O(\alpha_s)$ subdiagrams for the final π meson wave function.

By summing up all terms in Eqs. (21)–(23), one finds that the soft contributions in the limit $l\to 0$ from Figs. 3(c) and 4(f) cancel each other, while the remaining collinear contributions in the regions of $l\|p_1$ and $l\|p_2$ are of the form

$$G^{(1)}_{3c+3d+4f}(l\|p_1) = -\frac{\alpha_s C_F}{8\pi}[2\ln\delta_1]H^{(0)}(p_2^\mu),\tag{24}$$

$$G^{(1)}_{3c+3d+4f}(l\|p_2) = -\frac{\alpha_s C_F}{8\pi}[2\ln\delta_2]H^{(0)}(p_2^\mu).\tag{25}$$

The IR contributions to NLO twist-3 corrections to $H^{(0)}(x_1p_1^\mu)$ can be obtained in a similar way,

$$G^{(1)}_{3b}(l\|p_2) = -\frac{\alpha_s}{8\pi N_c}\left[1-\ln\frac{\delta_2}{x_1}\right]H^{(0)}(x_1p_1^\mu),\tag{26}$$

$$G^{(1)}_{3e}(l\|p_2) = -\frac{\alpha_s N_c}{8\pi}\left[\ln\frac{\delta_2}{x_1}(\ln x_2+1)\right]H^{(0)}(x_1p_1^\mu),\tag{27}$$

$$\begin{aligned}
G^{(1)}_{4a}(l\|p_1) = -\frac{\alpha_s N_c}{8\pi}&\left[\ln\delta_1(\ln x_1+1)-\ln x_2\left(\frac{3}{2}\ln x_1+1\right)\right.\\
&\left.+\frac{\pi^2}{12}+\frac{1}{8}\right]H^{(0)}(x_1p_1^\mu),
\end{aligned}\tag{28}$$

$$\begin{aligned}
G^{(1)}_{4c}(l\to 0) &= -\frac{\alpha_s}{8\pi N_c}\left[\ln\delta_1\ln\delta_2+\frac{\pi^2}{3}\right]H^{(0)}(x_1p_1^\mu),\\
G^{(1)}_{4c}(l\|p_1) &= -\frac{\alpha_s}{8\pi N_c}\left[\ln\delta_1\ln\frac{\delta_2}{x_1}+\frac{\pi^2}{6}\right]H^{(0)}(x_1p_1^\mu),\\
G^{(1)}_{4c}(l\|p_2) &= -\frac{\alpha_s}{8\pi N_c}\left[\ln\delta_2\ln\frac{\delta_1}{x_2}+\ln x_2(\ln x_2+\ln x_1)+\frac{\pi^2}{6}\right]H^{(0)}(x_1p_1^\mu),
\end{aligned}\tag{29}$$

$$G^{(1)}_{4e}(l\to 0)=\frac{\alpha_s}{8\pi N_c}\left[\ln\delta_1\ln\delta_2+\frac{\pi^2}{3}\right]H^{(0)}(x_1p_1^\mu),$$
$$G^{(1)}_{4e}(l\|p_1)=\frac{\alpha_s}{8\pi N_c}\left[\ln\delta_1\ln\delta_2+\ln\delta_1-\ln x_1+\frac{\pi^2}{6}+3\right]H^{(0)}(x_1p_1^\mu),$$
$$G^{(1)}_{4e}(l\|p_2)=\frac{\alpha_s}{8\pi N_c}\left[\ln\delta_1\ln\delta_2+\frac{3}{2}\ln x_1+\frac{\pi^2}{6}-\frac{7}{4}\right]H^{(0)}(x_1p_1^\mu). \quad (30)$$

Again, the soft parts from Figs. 4(c) and 4(e) cancel each other, while the remaining collinear contributions to the LO hard kernel $H^{(0)}(x_1p_1^\mu)$, after summing up the amplitudes as given in Eqs. (26)–(30), are the following:

$$G^{(1)}_{4a+4c+4e}(l\|p_1)=-\frac{\alpha_sC_F}{8\pi}[2\ln\delta_1(\ln x_1+1)]\times H^{(0)}(x_1p_1^\mu),$$
$$G^{(1)}_{3b+3e+4c+4e}(l\|p_2)=-\frac{\alpha_sC_F}{8\pi}[2\ln\delta_2(\ln x_2+1)]\times H^{(0)}(x_1p_1^\mu). \quad (31)$$

Note that we have dropped the constant terms in Eqs. (25) and (31), since we here consider the IR parts only. According to previous studies in Refs. [8–10], we know that these IR divergences could be absorbed into the NLO wave functions of the pion mesons. This point will become clear after we complete the calculations for the effective diagrams in Figs. 5 and 6. This absorption means that the k_T factorization is valid at the NLO level for the $\pi\gamma^*\to\pi$ process.

Without the reducible diagrams $G^{(1)}_{2a,2b,2c,2d,4b,4d}$, the summation for the NLO twist-3 contributions from all the irreducible QCD quark diagrams as illustrated by Figs. 2, 3, and 4 leads to the final result for $G^{(1)}$:

$$G^{(1)}=\frac{\alpha_sC_F}{8\pi}\left[\frac{29}{2}\left(\frac{1}{\varepsilon}+\ln\frac{4\pi\mu^2}{Q^2e^{\gamma_E}}\right)-2\ln\delta_1(\ln x_1+1)-2\ln\delta_2(\ln x_2+1)\right.$$
$$\left.-\frac{21}{8}\ln(x_1x_2)-\frac{23}{8}\ln x_1-\frac{1}{4}\ln^2x_2-\frac{9}{4}\ln x_2-\frac{3\pi^2}{16}+\frac{721}{32}\right]H^{(0)}(x_1p_1^\mu)$$
$$+\frac{\alpha_sC_F}{8\pi}\left[\frac{29}{2}\left(\frac{1}{\varepsilon}+\ln\frac{4\pi\mu^2}{Q^2e^{\gamma_E}}\right)-2\ln\delta_1-2\ln\delta_2-4\ln(x_1x_2)-5\ln x_1+\frac{\pi^2}{12}+\frac{\ln 2}{2}+23\right]H^{(0)}(p_2^\mu), \quad (32)$$

for $N_f=6$. The UV divergence in the above expression is the same one as in the pion electromagnetic form factor [9], which determines the renormalization-group (RG) evolution of the strong coupling constant α_s.

B. Convolution of the $O(\alpha_s)$ wave functions with the LO hard kernel

A basic argument of k_T factorization is that the IR divergences from the NLO corrections can also be absorbed into the nonperturbative wave functions which are universal. From this point, the convolution of the NLO wave functions and the LO hard kernel $H^{(0)}$ are computed, and the resultant IR part should cancel the IR divergences appeared in the NLO amplitude $G^{(1)}$ as given in Eq. (32).

The convolution of the NLO pion wave functions and the LO hard kernel are calculated in this subsection. In k_T factorization theorem, the $\Phi^{(1)}_{\pi,P}$ and $\Phi^{(1)}_{\pi,T}$ collect the $O(\alpha_s)$ effective diagrams for the twist-3 transverse momentum dependent (TMD) light-cone wave function $\Phi_{\pi,P}$ and $\Phi_{\pi,T}$, respectively [11,23]. In the $\pi\gamma^\star\to\pi$ process we calculate, only the $O(\alpha_s)$- order pseudoscalar component $\Phi^{(1)}_{\pi,P}$ of the final state pion, but both the $\Phi^{(1)}_{\pi,P}$ and $\Phi^{(1)}_{\pi,T}$ components of the initial pion should be convoluted with the LO hard kernel,

$$\Phi_{\pi,P}(x_1',k_{1T}';x_1,k_{1T})=\int\frac{dy^-}{2\pi}\frac{d^2y_T}{(2\pi)^2}e^{-ix_1'P_1^+y^-+i\mathbf{k}_{1T}'\cdot\mathbf{y}_T}\cdot\langle 0|\bar q(y)\gamma_5W_y(n_1)^\dagger I_{n_1;y,0}W_0(n_1)q(0)|\bar u(P_1-k_1)d(k_1)\rangle, \quad (33)$$

$$\Phi_{\pi,T}(x_1', k_{1T}'; x_1, k_{1T}) = \int \frac{dy^-}{2\pi}\frac{d^2y_T}{(2\pi)^2} e^{-ix_1' P_1^+ y^- + i\mathbf{k}_{1T}'\cdot\mathbf{y}_T} \cdot \langle 0|\bar{q}(y)\gamma_5(\not{n}_+\not{n}_- - 1)W_y(n_1)^\dagger I_{n_1;y,0} W_0(n_1) q(0)|\bar{u}(P_1 - k_1)d(k_1)\rangle, \tag{34}$$

$$\Phi_{\pi,P}(x_2, k_{2T}; x_2', k_{2T}') = \int \frac{dz^+}{2\pi}\frac{d^2z_T}{(2\pi)^2} e^{-ix_2' P_2^- z^+ + i\mathbf{k}_{2T}'\cdot\mathbf{z}_T} \cdot \langle 0|\bar{q}(z)W_z(n_2)^\dagger I_{n_2;z,0} W_0(n_2)\gamma_5 q(0)|u(P_2 - k_2)\bar{d}(k_2)\rangle, \tag{35}$$

where $y = (0, y^-, \mathbf{y}_T)$ and $z = (z_+, 0, \mathbf{z}_T)$ are the light-cone coordinates of the antiquark field $\bar{q}$ carrying the momentum faction x_i, respectively. The Wilson lines with the choice of $n_i^2 \neq 0$ to avoid the light-cone singularity [10,24] are defined as

$$W_y(n_1) = \mathrm{P}\exp\left[-ig_s\int_0^\infty d\lambda n_1\cdot A(y+\lambda n_1)\right], \tag{36}$$

$$W_z(n_2) = \mathrm{P}\exp\left[-ig_s\int_0^\infty d\lambda n_1\cdot A(z+\lambda n_2)\right], \tag{37}$$

where P is the path-ordering operator. The two Wilson lines $W_y(n_i)$ ($W_z(n_i)$) and $W_0(n_i)$ are connected by a vertical link $I_{n_i;y,0}$ ($I_{n_i;z,0}$) at infinity [25]. Then the additional light-cone singularities from the region where loop momentum $l\|n_-(n_+)$ [26] are regulated by the IR regulator $n_1^2 \neq 0$ and $n_2^2 \neq 0$. The scales $\xi_1^2 \equiv 4(n_1\cdot p_1)^2/|n_1^2| = Q^2|n_1^-/n_1^+|$ and $\xi_2^2 \equiv 4(n_2\cdot p_2)^2/|n_2^2| = Q^2|n_2^+/n_2^-|$ are introduced to describe the wave functions of the initial and final state pion respectively. It is important to emphasize that the variation of the above scales can be treated as a factorization scheme dependence, which entered the hard kernel when taking the difference of the quark diagrams in full QCD and the effective diagrams for the wave functions in NLO calculations. Recently, the above scheme-dependent rapidity logarithms were diminished by joint resummation [27] for B meson wave functions [28], and for the pion wave function and pion transition form factor [29]. In this paper we minimize the above scheme-dependent scales by adhering them to fixed n_1^2 and n_2^2.

The convolution of the $O(\alpha_s)$ initial state wave function as shown in Fig. 5 and $H^{(0)}$ over the integration variables x_1' and k_{1T}' is of the form

$$\Phi_\pi^{(1)} \otimes H^{(0)} \equiv \int dx_1' d^2\mathbf{k}_{1T}' \Phi_\pi^{(1)}(x_1, \mathbf{k}_{1T}; x_1', \mathbf{k}_{1T}') H^{(0)} \times (x_1', \mathbf{k}_{1T}'; x_2, \mathbf{k}_{2T}). \tag{38}$$

When making this convolution, the n_1 is chosen approximately as the vector n_- with a very small plus component n_1^+ to avoid the light-cone singularity. Note that the sign of n_1^- is positive while the sign of n_1^+ can be positive or negative for convenience. The results after making the convolution for each figure in Fig. 5 are given in the following with μ_f being the factorization scale:

$$\begin{aligned}
\Phi_{5a}^{(1)} \otimes H^{(0)} &= -\frac{\alpha_s C_F}{8\pi}\left[\frac{1}{\varepsilon} + \ln\frac{4\pi\mu_f^2}{\delta_1 Q^2 e^{\gamma_E}} + 2\right] H^{(0)},\\
\Phi_{5b}^{(1)} \otimes H^{(0)} &= -\frac{\alpha_s C_F}{8\pi}\left[\frac{1}{\varepsilon} + \ln\frac{4\pi\mu_f^2}{\delta_1 Q^2 e^{\gamma_E}} + 2\right] H^{(0)},\\
\Phi_{5c}^{(1)} \otimes H^{(0)} &\equiv 0,\\
\Phi_{5d}^{(1)} \otimes H^{(0)} &= \frac{\alpha_s C_F}{8\pi}\left[\frac{1}{\varepsilon} + \ln\frac{4\pi\mu_f^2}{\xi_1^2 e^{\gamma_E}} - \ln^2(\delta_1 r_Q) - 2\ln(\delta_1 r_Q) - \frac{\pi^2}{3} + 2\right] H^{(0)}(x_1 p_1^\mu),\\
\Phi_{5e}^{(1)} \otimes H^{(0)} &= \frac{\alpha_s C_F}{8\pi}\left[\ln^2\left(\frac{\delta_1 r_Q}{x_1}\right) + \pi^2\right] H^{(0)}(x_1 p_1^\mu),\\
\Phi_{5f}^{(1)} \otimes H^{(0)} &= \frac{\alpha_s C_F}{8\pi}\left[\frac{1}{\varepsilon} + \ln\frac{4\pi\mu_f^2}{\xi_1^2 e^{\gamma_E}} - \ln^2\left(\frac{\delta_1 r_Q}{x_1^2}\right) - 2\ln\left(\frac{\delta_1 r_Q}{x_1^2}\right) - \frac{\pi^2}{3} + 2\right] H^{(0)}(p_2^\mu),\\
\Phi_{5g}^{(1)} \otimes H^{(0)} &= \frac{\alpha_s C_F}{8\pi}\left[\ln^2\left(\frac{\delta_1 r_Q}{x_1^2}\right) - \frac{\pi^2}{3}\right] H^{(0)}(p_2^\mu),\\
(\Phi_{5h}^{(1)} + \Phi_{5i}^{(1)} + \Phi_{5j}^{(1)}) \otimes H^{(0)} &= \frac{\alpha_s C_F}{4\pi}\left[\frac{1}{\varepsilon} + \ln\frac{4\pi\mu_f^2}{Q^2 e^{\gamma_E}} - \ln\delta_{12}\right] H^{(0)}.
\end{aligned} \tag{39}$$

The dimensionless parameter $r_Q = Q^2/\xi_1^2$ is defined to simplify the expressions as given in the above equation. In Eq. (39) all the IR divergences are regulated by $\ln\delta_1$ in the convolution $\Phi_\pi^{(1)} \otimes H^{(0)}$. Figures 5(d),(e) just give the corrections to the LO hard kernel $H^{(0)}(x_1 p_1^\mu)$, while Figs. 5(f) and 5(g) provide the corrections to the LO hard kernel $H^{(0)}(p_2^\mu)$, because the gluon attaches to the Wilson line and the up external line in the former two subdiagrams [Figs. 5(d) and 5(e)], but attaches to the Wilson line and the down external line in the later two subdiagrams [Figs. 5(f) and 5(g)]. The corrections from Figs. 5(a) and 5(b) are canceled by those from Figs. 2(a) and 2(b). It is unnecessary to calculate the reducible subdiagram Fig. 5(c), since it will be canceled by Fig. 4(b) completely.

Only the three-point integral was involved in the convolution of $\Phi_{5d}^{(1)} \otimes H^{(0)}$ and $\Phi_{5f}^{(1)} \otimes H^{(0)}$, because there is no momenta flow into the LO hard kernel in these two sundiagrams. A four-point integral should been calculated in the convolution $\Phi_{5e}^{(1)} \otimes H^{(0)}$ because the momenta flow into the LO hard kernel and the $H^{(0)}(x_1 p_1^\mu)$ cancels the denominator. The convolution $\Phi_{5g}^{(1)} \otimes H^{(0)}$ involves a five-point integral due to the flow momenta and the correction to the LO hard kernel $H^{(0)}(p_2^\mu)$. After summing up all $O(\alpha_s)$ contributions in Fig. 5 except those from the reducible subdiagrams Figs. 5(a)–(c), we find

$$\Phi_\pi^{(1)} \otimes H^{(0)} = \frac{\alpha_s C_F}{8\pi}\left[\frac{3}{\varepsilon} + 3\ln\frac{4\pi}{e^{\gamma_E}} + 3\ln\frac{\mu_f^2}{Q^2} - 2\ln(\delta_1 r_Q)(\ln x_1 + 1) - 2\ln(x_1 x_2 r_Q) + \frac{2\pi^2}{3} - 2\right] H^{(0)}(x_1 p_1^\mu)$$
$$+ \frac{\alpha_s C_F}{8\pi}\left[\frac{3}{\varepsilon} + 3\ln\frac{4\pi}{e^{\gamma_E}} + 3\ln\frac{\mu_f^2}{Q^2} - 2\ln(\delta_1 r_Q) - 2\ln(x_1 x_2 r_Q) + 4\ln x_1 - \frac{2\pi^2}{3} - 2\right] H^{(0)}(p_2^\mu), \tag{40}$$

where $r_Q = Q^2/\xi_1^2$.

The convolution of the LO hard kernel $H^{(0)}$ and the NLO outgoing pion meson function $\Phi_\pi^{(1)}$ over the integration variables x_2' and k_{2T}' is

$$H^{(0)} \otimes \Phi_\pi^{(1)} \equiv \int dx_2' d^2\mathbf{k}_{2T}' H^{(0)}(x_1, \mathbf{k}_{1T}; x_2', \mathbf{k}_{2T}') \Phi_{\pi,P}^{(1)}(x_2', \mathbf{k}_{2T}'; x_2, \mathbf{k}_{2T}). \tag{41}$$

The unit vector n_2 is chosen approximately as n_+ with a very small minus component n_2^- to avoid the light-cone singularity in the convolution. Note that the sign of n_2^+ is positive as P_1^+ while the sign of n_2^- is arbitrary for convenience.

In Fig. 6 we draw all subdiagrams that provide $\mathcal{O}(\alpha_s)$ NLO corrections to the outgoing pion wave functions. Analogous to the case of Fig. 5, we here make the same evolutions for all subdiagrams in Fig. 6. The analytical results for each subdiagram of Fig. 6 are listed in the following with μ_f being the factorization scale:

$$H^{(0)} \otimes \Phi_{6a}^{(1)} = -\frac{\alpha_s C_F}{8\pi}\left[\frac{1}{\varepsilon} + \ln\frac{4\pi\mu_f^2}{\delta_2 Q^2 e^{\gamma_E}} + 2\right] H^{(0)},$$
$$H^{(0)} \otimes \Phi_{6b}^{(1)} = -\frac{\alpha_s C_F}{8\pi}\left[\frac{1}{\varepsilon} + \ln\frac{4\pi\mu_f^2}{\delta_2 Q^2 e^{\gamma_E}} + 2\right] H^{(0)},$$
$$H^{(0)} \otimes \Phi_{6c}^{(1)} \equiv 0,$$
$$H^{(0)} \otimes \Phi_{6d}^{(1)} = \frac{\alpha_s C_F}{8\pi}\left[\frac{1}{\varepsilon} + \ln\frac{4\pi\mu_f^2}{\xi_2^2 e^{\gamma_E}} - \ln^2(\delta_2\gamma_Q) - 2\ln(\delta_2\gamma_Q) - \frac{\pi^2}{3} + 2\right] H^{(0)}(x_1 p_1^\mu), \tag{42}$$

$$H^{(0)} \otimes \Phi_{6e}^{(1)} = \frac{\alpha_s C_F}{8\pi}\left[\ln^2\left(\frac{\delta_2 r_Q}{x_1}\right) + \pi^2\right] H^{(0)}(x_1 p_1^\mu),$$
$$H^{(0)} \otimes \Phi_{6f}^{(1)} = \frac{\alpha_s C_F}{8\pi}\left[\frac{1}{\varepsilon} + \ln\frac{4\pi\mu_f^2}{\xi_2^2 e^{\gamma_E}} - \ln^2\left(\frac{\delta_2 r_Q}{x_2^2}\right) - 2\ln\left(\frac{\delta_2 r_Q}{x_2^2}\right) - \frac{\pi^2}{3} + 2\right] H^{(0)}(p_2^\mu),$$
$$H^{(0)} \otimes \Phi_{6g}^{(1)} = \frac{\alpha_s C_F}{8\pi}\left[\ln^2\left(\frac{\delta_2 r_Q}{x_2^2}\right) - \frac{\pi^2}{3}\right] H^{(0)}(p_2^\mu),$$
$$H^{(0)} \otimes (\Phi_{6h}^{(1)} + \Phi_{6i}^{(1)} + \Phi_{6j}^{(1)}) = \frac{\alpha_s C_F}{4\pi}\left[\frac{1}{\varepsilon} + \ln\frac{4\pi\mu_f^2}{Q^2 e^{\gamma_E}} - \ln\delta_{12}\right] H^{(0)}, \tag{43}$$

where $r_Q = Q^2/\xi_1^2$. The most complex integral involved in our calculation for Fig. 6 is the four-point integral, since the relevant momentum fraction x_2' only appears in one propagator in the LO hard kernel $H^{(0)}$.

The total contributions from the convolution of the LO hard kernel $H^{(0)}$ and the NLO final pion meson wave function are obtained by summing up all contributions as listed in the above equation, and we dropped the contributions from those reducible subdiagrams $G^{(1)}(a, b, c)$. The summation from all irreducible subdiagrams of Fig. 6 leads to the final result:

$$H^{(0)} \otimes \Phi_\pi^{(1)} = \frac{\alpha_s C_F}{8\pi}\left[\frac{3}{\varepsilon} + 3\ln\frac{4\pi}{e^{\gamma_E}} + 3\ln\frac{\mu_f^2}{Q^2} - 2\ln(\delta_2 r_Q)(\ln x_2 + 1) - 2\ln(x_1 x_2 r_Q) + \frac{2\pi^2}{3} - 2\right] H^{(0)}(x_1 p_1^\mu)$$
$$+ \frac{\alpha_s C_F}{8\pi}\left[\frac{3}{\varepsilon} + 3\ln\frac{4\pi}{e^{\gamma_E}} + 3\ln\frac{\mu_f^2}{Q^2} - 2\ln(\delta_2 r_Q) - 2\ln(x_1 x_2 r_Q) + 4\ln x_2 - \frac{2\pi^2}{3} - 2\right] H^{(0)}(p_2^\mu), \quad (44)$$

where $r_Q = Q^2/\xi_1^2$.

C. The NLO twist-3 hard kernel

The IR-finite k_T-dependent NLO twist-3 hard kernel for the $\pi\gamma^* \to \pi$ form factor is derived by taking the difference between the contributions from the quark diagrams in full QCD and the contributions from the effective diagrams for pion wave functions [30]:

$$H^{(1)}(x_1, \mathbf{k}_{1T}; x_2, \mathbf{k}_{2T}) = G^{(1)}(x_1, \mathbf{k}_{1T}; x_2, \mathbf{k}_{2T}) - \int dx_1' d^2\mathbf{k}_{1T}' \Phi_\pi^{(1)}(x_1, \mathbf{k}_{1T}; x_1', \mathbf{k}_{1T}') H^{(0)}(x_1', \mathbf{k}_{1T}'; x_2, \mathbf{k}_{2T})$$
$$- \int dx_2' d^2\mathbf{k}_{2T}' H^{(0)}(x_1, \mathbf{k}_{1T}; x_2', \mathbf{k}_{2T}') \Phi_{\pi,P}^{(1)}(x_2', \mathbf{k}_{2T}'; x_2, \mathbf{k}_{2T}), \quad (45)$$

where $\Phi_\pi^{(1)}(x_1, \mathbf{k}_{1T}; x_1', \mathbf{k}_{1T}')$ include two parts, $\Phi_{\pi,P}^{(1)}(x_1, \mathbf{k}_{1T}; x_1', \mathbf{k}_{1T}')$ and $\Phi_{\pi,T}^{(1)}(x_1, \mathbf{k}_{1T}; x_1', \mathbf{k}_{1T}')$.

The bare coupling constant α_s in Eqs. (32), (40), and (44) can be rewritten as

$$\alpha_s = \alpha_s(\mu_f) + \delta Z(\mu_f)\alpha_s(\mu_f), \quad (46)$$

in which the counterterm $\delta Z(\mu_f)$ is defined in the modified minimal subtraction scheme. Inserting Eq. (46) into Eqs. (10), (32), (40), and (44) regularizes the UV poles in Eq. (45) through the term $\delta Z(\mu_f) H^{(0)}$, and then the UV poles in Eqs. (40) and (44) are regulated by the counterterm of the quark field and by an additional counterterm in the modified minimal subtraction scheme. The UV behavior of the NLO twist-3 contributions is the same as the NLO twist-2 ones, which satisfy the requirement of the universality of the pion wave functions.

Based on the above calculations, it is straightforward to write down the NLO twist-3 hard kernel $H^{(1)}$ for Fig. 1(a), assuming $\xi_1^2 \equiv \xi_2^2 \equiv Q^2$,

$$H^{(1)} = \frac{\alpha_s(\mu_f) C_F}{8\pi}\left[\frac{21}{2}\ln\frac{\mu^2}{Q^2} - 6\ln\frac{\mu_f^2}{Q^2} - \frac{53}{8}\ln(x_1 x_2) - \frac{23}{8}\ln x_1 - \frac{4}{9}\ln x_2 - \frac{1}{4}\ln^2 x_2 - \frac{137}{48}\pi^2 + \frac{337}{32}\right] H^{(0)}(x_1 p_1^\mu)$$
$$+ \frac{\alpha_s(\mu_f) C_F}{8\pi}\left[\frac{21}{2}\ln\frac{\mu^2}{Q^2} - 6\ln\frac{\mu_f^2}{Q^2} - 8\ln(x_1 x_2) - \ln x_1 + 4\ln x_2 - \frac{31}{12}\pi^2 + \frac{1}{2}\ln 2 + 11\right] H^{(0)}(p_2^\mu), \quad (47)$$

where μ and μ_f are the renormalization scale and factorization scale, respectively. Following the schemes in the NLO analysis of the $B \to \pi$ transition form factor at the leading twist [10], we here also set $\xi_2^2 = Q^2$ in order to obtain a simple expression as given in Eq. (47).

The additional double logarithm $\ln^2 x_1$, derived in the limit that the internal quark is on-shell due to the tiny momentum fraction x_1, should also be considered. It can be absorbed into the jet function $J(x_1)$ as in Refs. [14,15],

$$J^{(1)} H^{(0)} = -\frac{1}{2}\frac{\alpha_s(\mu_f) C_F}{4\pi}\left[\ln^2 x_1 + \ln x_1 + \frac{\pi^2}{3}\right] H^{(0)}(p_2^\mu), \quad (48)$$

where the factor $\frac{1}{2}$ reflects the different spin structure of the twist-3 and twist-2 parts. There exists no jet function $J(x_2)$ because the momentum fraction x_2 would not grow endpoint singularity. The NLO twist-3 hard kernel $H^{(1)}$ in Eq. (47) will become the following form after subtracting out the jet function in Eq. (48),

$$H^{(1)}(x_i, \mu, \mu_f, Q^2) \to H^{(1)} - J^{(1)} H^{(0)}$$
$$\equiv F_{\mathrm{T3,A1}}^{(1)}(x_i, \mu, \mu_f, Q^2) H^{(0)}(x_1 p_1^\mu) + F_{\mathrm{T3,A2}}^{(1)}(x_i, \mu, \mu_f, Q^2) H^{(0)}(p_2^\mu), \quad (49)$$

where the two factors of the NLO twist-3 contributions for Fig. 1(a) are of the form

$$F_{\mathrm{T3,A1}}^{(1)}(x_i, \mu, \mu_f, Q^2) = \frac{\alpha_s(\mu_f) C_F}{8\pi}\left[\frac{21}{2}\ln\frac{\mu^2}{Q^2} - 6\ln\frac{\mu_f^2}{Q^2} - \frac{53}{8}\ln(x_1 x_2) - \frac{23}{8}\ln x_1 - \frac{4}{9}\ln x_2 - \frac{1}{4}\ln^2 x_2 - \frac{137}{48}\pi^2 + \frac{337}{32}\right], \quad (50)$$

$$F^{(1)}_{\mathrm{T3,A2}}(x_i,\mu,\mu_f,Q^2)=\frac{\alpha_s(\mu_f)C_F}{8\pi}\left[\frac{21}{2}\ln\frac{\mu^2}{Q^2}-6\ln\frac{\mu_f^2}{Q^2}-8\ln(x_1x_2)+\ln^2x_1+4\ln x_2-\frac{27}{12}\pi^2+\frac{1}{2}\ln 2+11\right]. \quad (51)$$

The IR-finite and k_T dependent NLO hard kernel $H^{(1)}(\mu,\mu_f,x_i,Q^2)$ as given in Eq. (49) describe the NLO twist-3 contribution to the LO twist-3 hard kernel $H_a^{(0)}$ as given in Eq. (6) for the Fig. 1(a). One can obtain the NLO twist-3 corrections to the LO twist-3 hard kernel $H_b^{(0)}$, $H_c^{(0)}$, and $H_d^{(0)}$ for the other three subdiagrams Figs. 1(b)–(d), respectively, by simple replacements. For Fig. 1(b), for example, the two factors of the NLO twist-3 contributions $F^{(1)}_{\mathrm{T3,B1}}(x_i,\mu,\mu_f,Q^2)$ and $F^{(1)}_{\mathrm{T3,B2}}(x_i,\mu,\mu_f,Q^2)$ can be obtained from those in Eqs. (50) and (51) by simple replacements $x_1\leftrightarrow x_2$:

$$F^{(1)}_{\mathrm{T3,B1}}(x_i,\mu,\mu_f,Q^2)=\frac{\alpha_s(\mu_f)C_F}{8\pi}\left[\frac{21}{2}\ln\frac{\mu^2}{Q^2}-6\ln\frac{\mu_f^2}{Q^2}-\frac{53}{8}\ln(x_1x_2)-\frac{23}{8}\ln x_2-\frac{4}{9}\ln x_1-\frac{1}{4}\ln^2x_1-\frac{137}{48}\pi^2+\frac{337}{32}\right], \quad (52)$$

$$F^{(1)}_{\mathrm{T3,B2}}(x_i,\mu,\mu_f,Q^2)=\frac{\alpha_s(\mu_f)C_F}{8\pi}\left[\frac{21}{2}\ln\frac{\mu^2}{Q^2}-6\ln\frac{\mu_f^2}{Q^2}-8\ln(x_1x_2)+\ln^2x_2+4\ln x_1-\frac{27}{12}\pi^2+\frac{1}{2}\ln 2+11\right]. \quad (53)$$

We can also obtain the factors $F^{(1)}_{\mathrm{T3,C1}}$ and $F^{(1)}_{\mathrm{T3,C2}}$ for subdiagrams Fig. 1(c) by the replacements $x_1\to\bar{x}_1=1-x_1$ and $x_2\to\bar{x}_2=1-x_2$ from Eqs. (50) and (51). For Fig. 1(d), finally, one finds the factors $F^{(1)}_{\mathrm{T3,D1}}$ and $F^{(1)}_{\mathrm{T3,D2}}$ from those in Eqs. (50) and (51) by the replacements $x_1\to\bar{x}_2$ and $x_2\to\bar{x}_1$.

IV. NUMERICAL ANALYSIS

In this section, by employing the k_T factorization theorem, we will calculate the pion electromagnetic form factor $F^+(q^2)$ of the $\pi\gamma^*\to\pi$ process numerically. Besides the LO twist-2 and twist-3 contributions, the NLO twist-2 contribution as given in Ref. [9] and the NLO twist-3 contributions evaluated in this paper are all taken into account. We will compare the relative strength of the four parts numerically.

In order to compare our results directly with the theoretical predictions for the LO twist-2, LO twist-3, and NLO twist-2 contributions to pion form factor as presented in Ref. [9], we here first consider two different choices for the pion distribution amplitudes (DAs): Set A: the simple asymptotic pion DAs,

$$\phi_\pi^A(x)=\frac{3f_\pi}{\sqrt{6}}x(1-x),\quad \phi_\pi^P(x)=\frac{f_\pi}{2\sqrt{6}},\quad \phi_\pi^T(x)=\frac{f_\pi}{2\sqrt{6}}(1-2x), \quad (54)$$

with the pion decay constant $f_\pi=0.13$ GeV, and Set B: the nonasymptotic pion DAs, the same as those given in Eq. (39) of Ref. [9],

$$\phi_\pi^A(x)=\frac{3f_\pi}{\sqrt{6}}x(1-x)[1+0.16C_2^{\frac{3}{2}}(u)+0.04C_4^{\frac{3}{2}}(u)],$$
$$\phi_\pi^P(x)=\frac{f_\pi}{2\sqrt{6}}[1+0.59C_2^{\frac{1}{2}}(u)+0.09C_4^{\frac{1}{2}}(u)],$$
$$\phi_\pi^T(x)=\frac{f_\pi}{2\sqrt{6}}(1-2x)[1+0.019(1-10x+10x^2)], \quad (55)$$

where $u=1-2x$, and the Gegenbauer polynomials $C_{2,4}^{1/2,3/2}(u)$ can be found easily in Refs. [19,31].

In order to check the variations of the theoretical predictions induced by using different nonasymptotic pion DAs, we also consider the third choice of pion DAs, Set-C, which are the pion DAs popularly used in recent years, for example, in Refs. [32–34],

$$\phi_\pi^A(x)=\frac{3f_\pi}{\sqrt{6}}x(1-x)[1+a_2^\pi C_2^{\frac{3}{2}}(u)+a_4^\pi C_4^{\frac{3}{2}}(u)],$$
$$\phi_\pi^P(x)=\frac{f_\pi}{2\sqrt{6}}\left[1+\left(30\eta_3-\frac{5}{2}\rho_\pi^2\right)C_2^{\frac{1}{2}}(u)-3\left(\eta_3\omega_3+\frac{9}{20}\rho_\pi^2(1+6a_2^\pi)\right)C_4^{\frac{1}{2}}(u)\right],$$
$$\phi_\pi^T(x)=\frac{f_\pi}{2\sqrt{6}}(1-2x)\left[1+6\left(5\eta_3-\frac{1}{2}\eta_3\omega_3-\frac{7}{20}\rho_\pi^2-\frac{3}{5}\rho_\pi^2a_2^\pi\right)(1-10x+10x^2)\right], \quad (56)$$

where the Gegenbauer moments a_i^π, the parameters η_3,ω_3, and ρ_π are adopted from Refs. [19,31,32],

$$a_2^\pi=0.25,\quad a_4^\pi=-0.015,\quad \rho_\pi=m_\pi/m_0,$$
$$\eta_3=0.015,\quad \omega_3=-3.0, \quad (57)$$

with $m_\pi=0.13$, $m_0=1.74$ GeV. It is easy to see that the asymptotic pion DAs in Eq. (54) are just the first (leading) term of the nonasymptotic pion DAs as given in Eqs. (55) and (56). We will make numerical calculations by employing these three sets of pion DAs respectively, for the sake of comparison and for the examination of the effects of the shape of the pion DAs.

When both the LO twist-2 and LO twist-3 contributions are included, the LO form factor for the $\pi\gamma^\star \to \pi$ process can be written as [9,35]

$$F^+(Q^2)|_{\rm LO} = \frac{8}{9}\pi Q^2 \int dx_1 dx_2 \int b_1 db_1 b_2 db_2 \cdot \{x_1\phi_\pi^A(x_1)\phi_\pi^A(x_2) - 2r_\pi^2\phi_\pi^P(x_2)[(x_1-1)\phi_\pi^P(x_1) + (x_1+1)\phi_\pi^T(x_1)]\} \cdot \alpha_s(t)\cdot e^{-2S_\pi(t)}\cdot S_t(x_2)\cdot h(x_1,x_2,b_1,b_2), \quad (58)$$

where $r_\pi^2 = m_0^2/Q^2$, the first term $x_1\phi_\pi^A(x_1)\phi_\pi^A(x_2)$ leads to the LO twist-2 contribution, while the second term in the large bracket provides the LO twist-3 part. The k_T resummation factor $S_\pi(t)$ is adopted from Refs. [35,36],

$$S_\pi(\mu, b_i) = s\left(x_i\frac{Q}{\sqrt{2}}, b_i\right) + s\left(\bar{x}_i\frac{Q}{\sqrt{2}}, b_i\right) + 2\int_{1/b_i}^{\mu}\frac{d\bar{\mu}}{\bar{\mu}}r_Q(g(\bar{\mu})), \quad (59)$$

with $i = 1, 2$ for the initial and final π meson, respectively. The expressions of the function $s(Q', b)$ and the anomalous dimension γ_q can be found in Ref. [36]. The threshold resummation factor $S_t(x)$ in Eq. (58) is adopted from Ref. [12],

$$S_t(x) = \frac{2^{1+2c}\Gamma(3/2+c)}{\sqrt{\pi}\Gamma(1+c)}[x(1-x)]^c, \quad (60)$$

and we here set the parameter $c = 0.3$. The hard function $h(x_1, x_2, b_1, b_2)$ in Eq. (58) comes form the Fourier transformation and can be written as [9]

$$h(x_1,x_2,b_1,b_2) = K_0(\sqrt{x_1x_2}Qb_1)[\theta(b_1-b_2)I_0(\sqrt{x_2}Qb_2)K_0(\sqrt{x_2}Qb_1) + \theta(b_2-b_1)I_0(\sqrt{x_2}Qb_1)K_0(\sqrt{x_2}Qb_2)], \quad (61)$$

where J_0 is the Bessel function, and K_0, K_1, and I_0 are modified Bessel functions.

According to the discussions as presented in Ref. [9], we get to know that the relative strength of the NLO twist-2 contribution to the LO twist-2 one has a moderate dependence on the choice of the renormalization scale μ, the factorization scale μ_f, and the hard scale t. One can see from the curves in Fig. 6 of Ref. [9] that when one adopts the conventional choice of the scales [5], i.e.,

$$\mu = \mu_f = t = \max(\sqrt{x_1}Q, \sqrt{x_2}Q, 1/b_1, 1/b_2), \quad (62)$$

where the hard scale t is the largest energy scale in Fig. 1, the NLO twist-2 correction becomes less than 40% of the LO twist-2 contribution as $Q^2 > 7$ GeV^2, or less than 20% of the total LO contribution. This means that such a choice can minimize the NLO twist-2 correction to the form factors in consideration. We here also make the same choices as given in Eq. (62) in our numerical calculations of the NLO twist-2 and twist-3 contributions. For more details about the choice of μ, μ_f, and hard scale t, one can see Ref. [9].

When the LO twist-2, LO twist-3, NLO twist-2, and NLO twist-3 contributions to the pion form factors are all taken into account, the pion form factor $F^+(q^2)$ for $\pi\gamma^\star \to \pi$ process in the k_T factorization can be written as

$$F^+(Q^2)|_{\rm NLO} = \frac{8}{9}\pi Q^2 \int dx_1 dx_2 \int b_1 db_1 b_2 db_2 \cdot \{x_1\phi_\pi^A(x_1)\phi_\pi^A(x_2)\cdot[1 + F_{\rm T2}^{(1)}(x_i,t,Q^2)] - 2r_\pi^2 x_1\phi_\pi^P(x_2)[1 + \cdot F_{\rm T3}^{(1)}(x_i,t,Q^2)](\phi_\pi^P(x_1) + \phi_\pi^T(x_1)) + 2r_\pi^2\phi_\pi^P(x_2)[1 + \bar{F}_{\rm T3}^{(1)}(x_i,t,Q^2)]\cdot(\phi_\pi^P(x_1) - \phi_\pi^T(x_1))\}\cdot\alpha_s(t)\cdot e^{-2S_\pi(t)}\cdot S_t(x_2)\cdot h(x_1,x_2,b_1,b_2), \quad (63)$$

where the factor $F_{\rm T2}^{(1)}(x_i,t,Q^2)$ denotes the NLO twist-2 contribution as given in Ref. [9],

$$F_{\rm T2}^{(1)}(x_i,t,Q^2) = \frac{\alpha_s(t)C_F}{4\pi}\left[-\frac{3}{4}\ln\frac{t^2}{Q^2} - \ln^2 x_1 - \ln^2 x_2 + \frac{45}{8}\ln x_1\ln x_2 + \frac{5}{4}\ln x_1 + \frac{77}{16}\ln x_2 + \frac{1}{2}\ln 2 + \frac{5}{48}\pi^2 + \frac{53}{4}\right]. \quad (64)$$

The factors $F_{\rm T3}^{(1)}(x_i,t,Q^2)$ and $\bar{F}_{\rm T3}^{(1)}(x_i,t,Q^2)$ in Eq. (63) describe the NLO twist-3 contributions and have been defined in Eqs. (50) and (51). By making the same choice of scales (μ, μ_f, t) as the one in Eq. (62), these two factors become relatively simple,

$$F_{\rm T3}^{(1)}(x_i,t,Q^2) = \frac{\alpha_s(t)C_F}{4\pi}\left[\frac{9}{4}\ln\frac{t^2}{Q^2} - \frac{53}{16}\ln x_1x_2 - \frac{23}{16}\ln x_1 - \frac{2}{9}\ln x_2 - \frac{1}{8}\ln^2 x_2 - \frac{137}{96}\pi^2 + \frac{337}{64}\right], \quad (65)$$

$$\bar{F}^{(1)}_{\rm T3}(x_i,t,Q^2)=\frac{\alpha_s(t)C_F}{4\pi}\left[\frac{9}{4}\ln\frac{t^2}{Q^2}-4\ln(x_1x_2)+\frac{1}{2}\ln^2x_1+2\ln x_2-\frac{27}{24}\pi^2+\frac{1}{4}\ln 2+\frac{11}{2}\right]. \quad (66)$$

By using the three sets of pion distribution amplitudes $\phi_\pi^{A,P,T}(x)$ as given in Eqs. (54), (55), and (56), respectively, and fixing the scales as in Eq. (62), we calculate the four different LO and NLO contributions to the pion form factors and show the theoretical predictions in Tables I and II, and in Figs. 7–10, respectively.

In Table I, we list the theoretical predictions for the four kinds of contributions: the LO twist-2, LO twist-3, NLO twist-2, and NLO twist-3 contributions to the pion form factors $Q^2F^+(Q^2)$ for fixed values of $Q^2=(1,3,5,7,10,100)$ GeV^2. In the numerical calculations, three sets of different choices of pion DAs are used, respectively, with the labels of Set-A, Set-B, and Set-C.

In order to compare the relative strengths of different contributions directly, we define the following four ratios,

$$R_1=\frac{F^+_{\rm NLO\text{-}T2}(Q^2)}{F^+_{\rm LO\text{-}T2}(Q^2)},\quad R_2=\frac{F^+_{\rm NLO\text{-}T3}(Q^2)}{F^+_{\rm LO\text{-}T3}(Q^2)},$$
$$R_3=\frac{F^+_{\rm NLO}(Q^2)}{F^+_{\rm LO}(Q^2)},\quad R_4=\frac{F^+_{\rm NLO}(Q^2)}{F^+_{\rm NLO}(Q^2)+F^+_{\rm LO}(Q^2)}, \quad (67)$$

where R_1 (R_2) measures the ratio between NLO twist-2 (twist-3) and LO twist-2 (twist-3) contribution, R_3 describes the relative strength between the NLO contribution and the LO ones, and finally R_4 is the ratio of the NLO contribution over the total contribution, with all four parts, LO plus NLO contributions. In Table II, we present the numerical values of the ratios of the different kinds of contributions to $F^+(Q^2)$ for fixed values of $Q^2=(1,3,5,7,10,100)$ GeV^2 and for three different sets of the pion DAs, respectively.

In Fig. 7, we show the Q^2 dependence of the various contributions to the pion form factors from different orders and twists for $1\le Q^2\le 100$ GeV^2, by using the asymptotic pion DAs as given in Eq. (54) and setting $\mu=\mu_f=t$. Figure 7(b) shows the enlargement of Fig. 7(a) in the low-Q^2 region: $1\le Q^2\le 10$ GeV^2. The experimental data shown in Fig. 7(b) are taken from Refs. [37,38]. The Figs. 8 and 9 also show the Q^2 dependence of the various contributions to the pion form factors, but using the nonasymptotic pion DAs as given in Eqs. (55) and (56) instead of the asymptotic ones in Eq. (54). In Fig. 10, we show the Q^2 dependence of the four ratios $R_{1,2}$ and $R_{3,4}$ for $1\le Q^2\le 100$ GeV^2, assuming $c=0.3$ and $\mu=\mu_f=t$ and employing the three different sets of the pion DAs.

From the theoretical predictions for the pion form factors from different orders and twists, as listed in Tables I and II, and illustrated in Figs. 7–10, one can have the following observations:

(i) For the LO twist-2 and NLO twist-2 contributions to the pion form factors $F^+(Q^2)$ obtained in this work agree very well with those presented in Ref. [9] when the same Set-A and Set-B pion DAs are used, as can be seen easily from the numerical results in Tables I and II, as well as in Figs. 7–9. Even when the Set-C pion DAs as given in Eq. (56) were used, the theoretical predictions for the LO twist-2 and NLO twist-2 contributions are still well consistent with those in Ref. [9], since the twist-2 $\phi_\pi^A(x)$ in Eqs. (55) and (56) are only slightly different. By using $a_2^\pi=0.25$ and $a_4^\pi=-0.015$, we find from Eq. (56) directly that

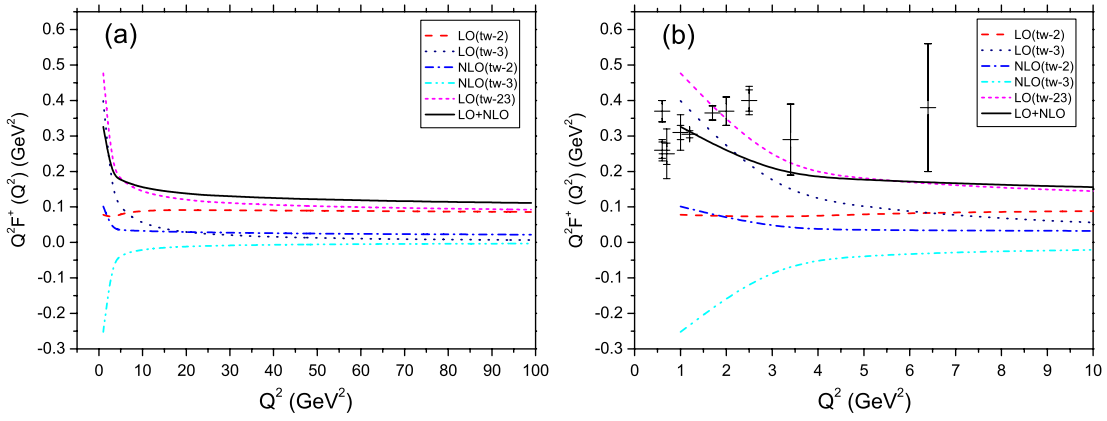

FIG. 7 (color online). Contributions to $Q^2F^+(Q^2)$ from different orders and twists, using the asymptotic pion DAs as given in Eq. (54). Figure 7(a) shows the Q^2 dependence for $1\le Q^2\le 100$ GeV^2, while 7(b) is the enlargement of 7(a) in the low-Q^2 region, $1\le Q^2\le 10$ GeV^2. The experiment data in 7(b) are taken from Refs. [37,38].

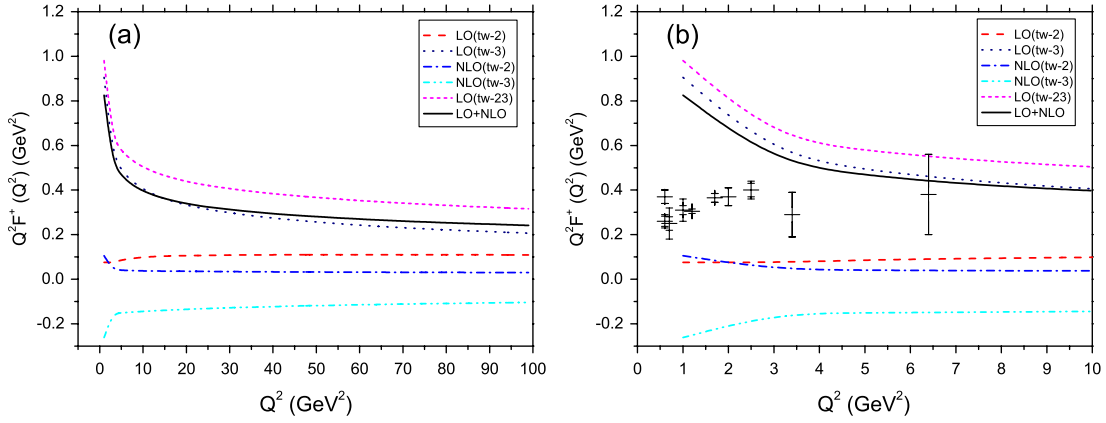

FIG. 8 (color online). The same as Fig. 7, but using the nonasymptotic pion DAs as given in Eq. (55).

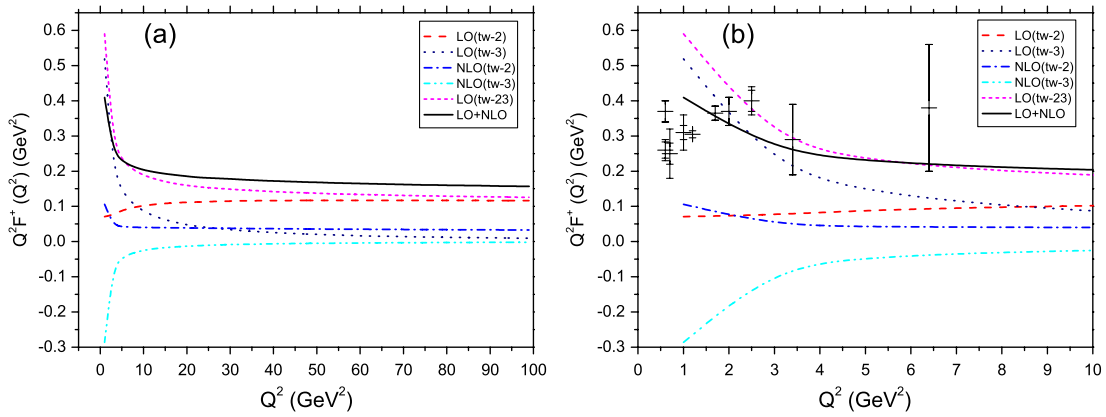

FIG. 9 (color online). The same as Fig. 7, but using the nonasymptotic pion DAs as given in Eq. (56).

$$\phi_\pi^A(x) = \frac{f_\pi}{2\sqrt{6}}[1 + 0.25C_2^{\frac{3}{2}}(u) - 0.015C_4^{\frac{3}{2}}(u)]. \quad (68)$$

The coefficient of the second term is $a_2^\pi = 0.25$, close to the 0.16 in the $\phi_\pi^A(x)$ in Eq. (55).

(ii) For the LO twist-3 and NLO twist-3 contributions, one can see from the numerical results in Table I and the cures in Figs. 7–9 that these two contributions are rather similar to each other in both the magnitude and the shape when Set-A and Set-C pion DAs are used, respectively. When the Set-B pion DAs as given in Eq. (55) are employed, however, the corresponding theoretical predictions for both the LO twist-3 and NLO twist-3 contributions become rather different from those obtained by using the Set-C pion DAs. The reason

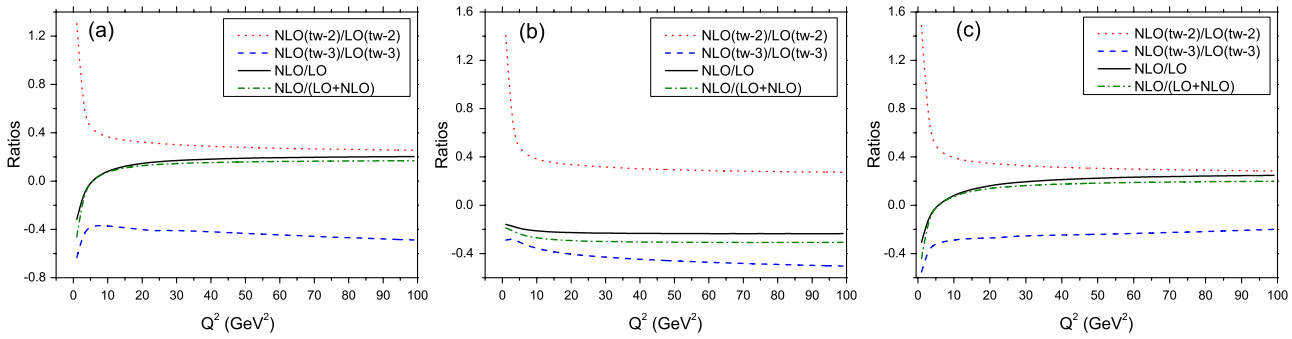

FIG. 10 (color online). Ratios of the NLO corrections over the LO contributions to the pion form factor, assuming $\mu = \mu_f = t$. (a) the asymptotic pion DAs in Eq. (54) are used, (b) the nonasymptotic DAs in Eq. (55) are used, and (c) the nonasymptotic DAs in Eq.(56) are used.

TABLE I. The theoretical predictions for contributions to $Q^2F^+(Q^2)$ from different orders and twists, for $Q^2 = (1, 3, 5, 7, 10, 100)$ GeV^2 and for different cases, i.e., using different sets of pion DAs, respectively.

$Q^2F^+(Q^2)$	DAs	1	3	5	7	10	100
LO T-2	Set-A	0.078	0.070	0.080	0.085	0.089	0.086
	Set-B	0.075	0.075	0.086	0.093	0.098	0.109
	Set-C	0.071	0.076	0.089	0.095	0.102	0.116
NLO-T2	Set-A	0.102	0.039	0.035	0.034	0.033	0.022
	Set-B	0.106	0.044	0.040	0.039	0.037	0.030
	Set-C	0.106	0.047	0.043	0.041	0.040	0.033
LO-T3	Set-A	0.399	0.141	0.099	0.076	0.056	0.007
	Set-B	0.905	0.558	0.491	0.447	0.405	0.207
	Set-C	0.519	0.206	0.145	0.113	0.087	0.010
NLO-T3	Set-A	−0.252	−0.059	−0.037	−0.028	−0.021	−0.003
	Set-B	−0.261	−0.155	−0.151	−0.148	−0.144	−0.104
	Set-C	−0.286	−0.073	−0.046	−0.034	−0.025	−0.002
Full LO	Set-A	0.476	0.211	0.179	0.160	0.145	0.092
	Set-B	0.981	0.633	0.571	0.540	0.504	0.316
	Set-C	0.590	0.282	0.234	0.209	0.189	0.126
LO + NLO	Set-A	0.326	0.190	0.176	0.166	0.156	0.111
	Set-B	0.825	0.522	0.466	0.431	0.397	0.242
	Set-C	0.409	0.256	0.230	0.216	0.204	0.157

is that there is a clear difference for the twist-3 DAs $\phi_\pi^P(x)$ and $\phi_\pi^T(x)$ in Eqs. (55) and (56), specifically for $\phi_\pi^T(x)$. Using the Gegenbauer moments and other input parameters as given in Eq. (57), we find numerically that

$$\phi_\pi^P(x) = \frac{f_\pi}{2\sqrt{6}}[1 + 0.43C_2^{\frac{1}{2}}(u) + 0.11C_4^{\frac{1}{2}}(u)],$$
$$\phi_\pi^T(x) = \frac{f_\pi}{2\sqrt{6}}(1-2x)[1 + 0.56(1 - 10x + 10x^2)]. \quad (69)$$

One can see that the coefficients (0.43,0.11) of $\phi_\pi^P(x)$ in Eq. (69) are close to (0.59,0.09) in Eq. (55), but the coefficient 0.56 of $\phi_\pi^T(x)$ in Eq. (69) is much larger than 0.019 in Eq. (55). Because the coefficient 0.019 is too small, the twist-3 nonasymptotic $\phi_\pi^T(x)$ as given in Eq. (55) is in fact the same one as the asymptotic $\phi_\pi^T(x)$ as given in Eq. (54). This is a little unreasonable in our opinion.

(iii) For the LO twist-2 contribution $F^+_{\text{LO-T2}}(Q^2)$, the theoretical prediction remains stable in the whole range of $1 \le Q^2 \le 100$ GeV^2 when asymptotic $\phi^A(x)$ is used, while it becomes a little bit large

TABLE II. The ratios of the different contributions or their combinations as defined in Eq. (67), for $Q^2 = (1, 3, 5, 7, 10, 100)$ GeV^2, respectively.

Ratios	DAs	1	3	5	7	10	100
R_1	Set-A	1.303	0.549	0.440	0.398	0.367	0.256
	Set-B	1.406	0.595	0.467	0.418	0.382	0.273
	Set-C	1.488	0.616	0.481	0.430	0.393	0.284
R_2	Set-A	−0.633	−0.423	−0.376	−0.368	−0.372	−0.487
	Set-B	−0.288	−0.277	−0.307	−0.331	−0.356	−0.503
	Set-C	−0.552	−0.356	−0.319	−0.302	−0.288	−0.199
R_3	Set-A	−0.316	−0.099	−0.012	0.036	0.080	0.203
	Set-B	−0.158	−0.174	−0.191	−0.202	−0.212	−0.235
	Set-C	−0.306	−0.094	−0.016	0.032	0.080	0.247
R_4	Set-A	−0.462	−0.110	−0.013	0.035	0.074	0.169
	Set-B	−0.188	−0.211	−0.237	−0.254	−0.269	−0.307
	Set-C	−0.441	−0.103	−0.016	0.031	0.074	0.198

along with the increase of Q^2 when the other two sets of pion DAs are employed, since the twist-2 $\phi_\pi^A(x)$ in Eqs. (55) and (56) are very similar to each other.

(iv) For the NLO twist-2 contribution, the value of $Q^2 F^+_{\text{NLO-T2}}(Q^2)$ becomes smaller rapidly in the low-Q^2 region, say $1 \le Q^2 \le 3$ GeV^2, and then decreases slowly from ~0.044 to 0.030 along with the increase of Q^2 from 3 to 100 GeV^2. The ratio R_1 is changing from ~60% for $Q^2 = 3$ to ~26% for $Q^2 = 100$ GeV^2.

(v) For the LO twist-3 contribution, the theoretical predictions for $Q^2 F^+_{\text{LO-T3}}(Q^2)$ obtained by using the Set-C pion DAs are about 15% larger than those obtained when the asymptotic $\phi_\pi^{P,T}$ are used, but much smaller than the ones from the Set-B pion DAs. The reason is of course the special choice of $\phi_\pi^T(x)$ in the Set-B pion DAs. In the low-Q^2 region of $Q^2 < 10$ GeV^2, the LO twist-3 contribution becomes small rapidly. From the numbers in Table I for the case of the Set-C pion DAs, one can see that the ratio between the LO twist-3 and LO twist-2 contribution is approximately 7.3,1.6,0.9 for $Q^2 = 1, 5, 10$ GeV^2, respectively. This is rather different from the behavior when the Set-B pion DAs are used, in which the LO twist-3 part is always larger than the LO twist-2 contribution by a factor ≥ 4.1.

(vi) For the NLO twist-3 contribution, the theoretical predictions for $Q^2 F^+_{\text{NLO-T3}}(Q^2)$ has an opposite sign with its counterpart $Q^2 F^+_{\text{NLO-T2}}(Q^2)$ and largely canceled each other. The NLO twist-3 contribution calculated by using the Set-A and Set-C pion DAs are similar in size (the difference is around 10%) in the whole range of Q^2 and become smaller rapidly along with the increase of Q^2, as illustrated by the lowest dot-dash curves in Figs. 7 and 9. The $Q^2 F^+_{\text{NLO-T3}}(Q^2)$ from the Set-B pion DAs is similar in size with those for other two cases at the starting point $Q^2 = 1$ GeV^2, but remain basically stable in the range of $Q^2 > 3$ GeV^2.

(vii) The ratio R_1 from the three different sets of pion DAs has similar value and Q^2 dependence, as illustrated by the upper dot curves in Fig. 10. The other three ratios $R_{2,3,4}$ as shown in Figs. 10(a) and 10(c) are also similar in size and in their Q^2 dependence, but rather different from those obtained by using the Set-B pion DAs. The ratio R_2 in Fig. 10(c), for example, is changing from −0.552 for $Q^2 = 1$ to −0.199 for $Q^2 = 100$ GeV^2, while the ratio R_2 in Fig. 10(b) changes its value from −0.288 for $Q^2 = 1$ to −0.503 for $Q^2 = 100$ GeV^2.

(viii) When the Set-C pion DAs are used, one can see from Table II and Fig. 10(c) that (a) at twist-2 level, the NLO twist-2 contribution can provide a strong enhancement to the LO twist-2 part, from 30% to 60% in the range of $3 < Q^2 \le 100$ GeV^2, (b) at twist-3 level, the NLO twist-3 contribution is about 30% of the LO twist-3 part in magnitude in the range of $3 < Q^2 \le 10$ GeV^2, but has an opposite sign with its LO counterpart in the whole range of Q^2, which leads to a partial cancelation of the LO and NLO twist-3 contributions.

(ix) Because of the strong cancelation between the NLO twist-2 and NLO twist-3 contributions, the total NLO contribution to pion form factor $F^+(Q^2)$ becomes small in size with respect to the total LO part, from about −31% for $Q^2 = 1$ to ~25% for $Q^2 = 100$ GeV^2 when the Set-C pion DAs are used. The ratio R_3 changes its sign at the point $Q^2 \sim 6$ GeV^2, as shown by the solid curve in Fig. 10(c). When the Set-B pion DAs are used, however, the ratio R_3 is always negative and keep stable in size for the whole range of Q^2.

V. CONCLUSION

In this paper, we made the first calculation for the NLO twist-3 contributions to the pion electromagnetic form factor for the $\pi\gamma^* \to \pi$ process, by employing the k_T factorization theorem and using the nonasymptotic pion distribution amplitudes: the leading twist-2 $\phi_\pi^A(x)$ and the twist-3 $\phi_\pi^{P,T}(x)$.

The UV divergences at the NLO twist-3 level are found to be the same ones as the NLO twist-2 part, which confirms the universality of the nonperturbative wave functions. These UV divergences are renormalized into the coupling constants and quark fields. Both the soft and collinear divergences in the NLO QCD quark diagrams and in the NLO effective diagrams for pion wave functions are regulated by the off-shell momentum k_T^2 of the light quark. The soft divergences cancels themselves in the quark diagrams and the collinear divergences cancels between the QCD quark diagrams and the effective diagrams at twist-3, in cooperation with the cancelation at the leading twist-2 [9], verified the validity of the k_T factorization for the exclusive decays at the NLO level. The large double logarithm $\ln^2 x_i$ in the NLO hard kernel are strongly suppressed by the Sudakov factor, then the NLO corrections are under control.

From the analytical calculations we obtained two factors $F^{(1)}_{\text{T3}}(x_i, t, Q^2)$ and $\bar{F}^{(1)}_{\text{T3}}(x_i, t, Q^2)$, which describe directly the NLO twist-3 contributions to the pion form factors $F^+(Q^2)$ as shown in Eq. (63). From the numerical results and phenomenological analysis, we found the following points:

(i) For the LO twist-2, twist-3, and NLO twist-2 contributions, our results agree very well with those as given in the previous work [9] for both the magnitude and the Q^2 dependence of the individual part.

(ii) The newly calculated NLO twist-3 contribution, which is negative in sign and will interfere

destructively with the NLO twist-2 part, leaves a relatively small total NLO contribution, which can result in roughly $\pm 20\%$ corrections to the total LO contribution in almost all considered ranges of Q^2.

(iii) The theoretical predictions for $Q^2F^+(Q^2)$ in the low-Q^2 region agree well with currently available data. The inclusion of NLO contributions results in a better agreement between the theory and the experiments.

(iv) The theoretical predictions for the pion form factors obtained by employing the k_T factorization theorem have a moderator dependence on the form and the shape of the pion distribution amplitudes, this is the main source of the theoretical uncertainty.

ACKNOWLEDGEMENTS

The authors would like to thank Hsiang-nan Li, Cai-Dian Lu, Xin Yu, Yu-Ming Wang, and Yue-Long Shen for collaboration and valuable discussions. This work is supported by the National Natural Science Foundation of China under Grants No. 10975074 and No. 11235005 and by the Project on Graduate Student Education and Innovation of Jiangsu Province under Grant No. CXZZ13-0391.

[1] J. Botts and G. Sterman, Nucl. Phys. **B 325**, 62 (1989); H. N. Li and G. Sterman, Nucl. Phys. **B 381**, 129 (1992); T. Huang and Q. X. Shen, Z. Phys. C **50**, 139 (1991); F. G. Cao, T. Huang and C. W. Luo, Phys. Rev. D **52**, 5358 (1995).
[2] J. C. Collins and R. K. Ellis, Nucl. Phys. **B 360**, 3 (1991).
[3] H. N. Li and H. L. Yu, Phys. Rev. Lett. **74**, 4388 (1995); Phys. Lett. B **353**, 301 (1995); Phys. Rev. D **53**, 2480 (1996).
[4] Y. Y. Keum, H. N. Li, and A. I. Sanda, Phys. Lett. B **504**, 6 (2001); Y. Y. Keum, H. N. Li and A. I. Sanda, Phys. Rev. D **63**, 054008 (2001).
[5] C. D. Lü, K. Ukai, and M. Z. Yang, Phys. Rev. D **63**, 074009 (2001).
[6] S. Catani, M. Ciafaloni, and F. Hautmann, Phys. Lett. B **242**, 97 (1990); Nucl. Phys. **B 366**, 135 (1991).
[7] J. P. Ralston and B. Pire, Phys. Rev. Lett. **65**, 2343 (1990).
[8] S. Nandi and H. N. Li, Phys. Rev. D **76**, 034008 (2007).
[9] H. N. Li, Y. L. Shen, Y. M. Wang, and H. Zou, Phys. Rev. D **83**, 054029 (2011).
[10] H. N. Li, Y. L. Shen, and Y. M. Wang, Phys. Rev. D **85**, 074004 (2012).
[11] H. N. Li, Phys. Rev. D **64**, 014019 (2001).
[12] T. Kurimoto, H. N. Li, and A. I. Sanda, Phys. Rev. D **65**, 014007 (2001).
[13] C. D. Lü and M. Z. Yang, Eur. Phys. J. C **23**, 275 (2002).
[14] H. N. Li, Phys. Rev. D **66**, 094010 (2002).
[15] H. N. Li, Phys. Lett. B **555**, 197 (2003).
[16] T. Altinoluk, B. Pire, L. Szymanowski and S. Wallon, J. High Energy Phys. 10 (2012) 049.
[17] V. M. Braun and I. E. Filyanov, Z. Phys. C **48**, 239 (1990).
[18] P. Ball, J. High Energy Phys. 01 (1999) 010.
[19] P. Ball, V. M. Braun and A. Lenz, J. High Energy Phys. 05 (2006) 004; P. Ball, V. M. Braun, Y. Koike, and K. Tanaka, Nucl. Phys. **B 529**, 323 (1998); P. Ball, J. High Energy Phys. 09 (1998) 005.
[20] Y. C. Chen and H. N. Li, Phys. Rev. D **84**, 034018 (2011).
[21] W. Siegel, Phys. Lett. **84B**, 193 (1979).
[22] B. W. Harris and J. F. Owens, Phys. Rev. D **65**, 094032 (2002).
[23] M. Nagashima and H. N. Li, Eur. Phys. J. C **40**, 395 (2005).
[24] J. P. Ma and Q. Wang, J. High Energy Phys. 01 (2006) 067; Phys. Lett. B **642**, 232 (2006).
[25] X. Ji and F. Yuan, Phys. Lett. B **543**, 66 (2002).
[26] J. C. Collins, Acta Phys. Pol. **B24**, 3103 (2003).
[27] H. N. Li, arXiv:1308.0413.
[28] H. N. Li, Y. L. Shen, and Y. M. Wang, J. High Energy Phys. 02 (2013) 008.
[29] H. N. Li, Y. L. Shen, and Y. M. Wang, J. High Energy Phys. 01 (2014) 004.
[30] M. Nagashima and H. N. Li, Phys. Rev. D **67**, 034001 (2003).
[31] P. Ball and R. Zwicky, Phys. Rev. D **71**, 014015 (2005).
[32] H. N. Li, S. Mishima, and A. I. Sanda, Phys. Rev. D **72**, 114005 (2005).
[33] H. S. Wang, X. Liu, Z. J. Xiao, L. B. Guo, and C. D. Lü, Nucl. Phys. **B 738**, 243 (2006); Z. J. Xiao, Z. Q. Zhang, X. Liu, and L. B. Guo, Phys. Rev. D **78**, 114001 (2008).
[34] Z. J. Xiao, W. F. Wang, and Y. Y. Fan, Phys. Rev. D **85**, 094003 (2012); W. F. Wang and Z. J. Xiao, Phys. Rev. D **86**, 114025 (2012); Y. Y. Fan, W. F. Wang, S. Cheng, and Z. J. Xiao, Phys. Rev. D **87**, 094003 (2013).
[35] Z. T. Wei and M. Z. Yang, Phys. Rev. D **67**, 094013 (2003).
[36] H. N. Li and B. Tseng, Phys. Rev. D **57**, 443 (1998).
[37] C. J. Bebek *et al.*, Phys. Rev. D **17**, 1693 (1978).
[38] G. M. Huber *et al.* (Jefferson Lab Collaboration), Phys. Rev. C **78**, 045203 (2008).